Discrete angle radiative transfer in a multifractal medium

Anthony Davis

Shaun Lovejoy

McGill University, Physics Department
3600 University St., Montreal (Qc.), H3A 2T8, CANADA

Daniel Schertzer

Météorologie Nationale, EERM/CRMD
2 Av. Rapp, 75007, Paris, FRANCE

ABSTRACT

A simplified (discrete angle or "DA") radiative transfer theory is presented as a computationally and conceptually advantageous alternative to standard (continuous angle) theory: its use is justified since these theories generally predict the same radiative scaling behavior whereas diffusion and independent pixel approximations do not. After briefly reviewing the basic ideas of random fractal geometry and multifractal cascade theory, we present some of our recent two-dimensional DA numerical simulations of transfer through a specific log-normal multifractal cloud model where the radiation fields are spatially resolved on a 1024x1024 point grid. Using this database, we demonstrate (i) how in inhomogeneous transfer problems horizontal fluxes work in quite subtle ways to create dramatic overall differences with homogeneous predictions for the same amount of scattering material, and (ii) how strongly multiple scattering can smooth extremely singular density fields. Furthermore, both of these effects are enhanced by increasing optical thickness which can be viewed as a measure of the strength of the nonlinear coupling between the density and radiance fields. Finally, we discuss some basic inequalities that arise between the various ways of computing overall (spatially averaged) response to illumination.

1. BACKGROUND AND OVERVIEW

In a recent series of papers,[1,2,3] we have given general, numerical and analytical arguments that global radiative responses such as transmittance (T) or reflectance (R) for conservative scattering and media that are invariant under overall changes of scale must vary algebraically with asymptotically large optical thickness ($\overline{\tau} \gg 1$), e.g., $T \approx h_T \overline{\tau}^{-\nu_T}$, where $\overline{\cdot}$ designates spatial averaging. If the scale invariance is only a statistical symmetry of the system (as in realistic models), then ensemble averages $\langle\cdot\rangle$ must also be taken. We examined homogeneous but horizontally finite media as well as a very simple deterministic monofractal cloud model (Fig. 1, below) in open[3] and cyclical[4] horizontal boundary conditions; our results show that the exponents are phase function independent in general and exhibit systematic differences with their homogeneous counterpart (which is 1), as well as sensitivity to the choice of physical transport theory (in inhomogeneous enough media). The finding that $\nu_{T,inhomo} < \nu_{T,homo} = 1$ provides a simple explanation of the cloud "albedo paradox"[5] which expresses the fact that it is impossible to reconcile the Earth's average albedo (≈ 0.3) and cloud cover ($\approx 50\%$) with the –still routinely used– homogeneous plane-parallel models and the independently known cloud optical thicknesses. The latter are highly variable but, generally speaking, $\overline{\tau}$ is several times $\tau_{eff} \approx 10$, the value predicted by the standard models for typical cloud (albedo ≈ 0.6) using an asymmetry factor $g \approx 0.85$, the average cosine of the (Mie) scattering angle for the observed (Diermenjian's "C1") droplet size distribution. A random version of the fractal cloud model in d = 3 was used to show[6] that sufficiently high $\langle\overline{\tau}/\tau_{eff}\rangle$ ratios can be obtained with cloud- (L) to homogeneity- (l_0) scale ratios ($\lambda = L/l_0$) as small as 32 at values of the "intermittancy" parameter that are quite consistent with those quoted in the turbulence literature. This is not a coincidence since the use of fractal geometry in cloud radiation studies was largely motivated in the first place by its close connection with turbulence theory as well as the successes of early (mono)fractal analyses[7] and syntheses[8] of the cloud and rain fields.

In the following section, we present the necessary elements of Discrete Angle (DA) radiative transfer used, for simplicity, in the numerical simulations (presented in section 4); this includes an improved similarity argument for why we expect in general different exponents for different transport theories, namely, exact transfer versus the diffusion- and "independent pixel"[9] (IP) approximations. IPs is a quite standard approach to radiation transport in inhomogeneous systems that treats the distribution of

density in every column as a separate plane-parallel transport problem (which is effectively 1-D), thus net horizontal fluxes that mediate radiation from one column to its neighbors are totally neglected; it has previously been applied to multifractals numerically and analytically.[10] In section 3, monofractal cloud models are defined from the standpoint of turbulent cascade phenomenology; they are immediately generalized to- and contrasted with their more interesting multifractal counterparts, introducing the necessary formalism on the way. In section 4, we describe the specific simulation and the methodology used in our new numerical results on the fully resolved internal radiation fields which we present and discuss. Finally (section 5), we draw our conclusions on the overwhelming (but subtle) importance of net horizontal fluxes –which IP approximations totally fail to capture– and discuss the most obvious meteorological implications.

2. DISCRETE ANGLE RADIATIVE TRANSFER - FUNDAMENTALS

2.1. DA multiple scattering as a special case of the standard continuous angle formulation

A very slight change in notation allows the standard (d=3) radiative transfer equation[11] with multiple scattering sources to be applicable to two spatial dimensions. Let $I_\theta(\mathbf{x})$ denotes the radiance at position $\mathbf{x}$ propagating into direction $\mathbf{u}(\theta)$, then we have:

$$\mathbf{u}\cdot\nabla I_{\mathbf{u}} = -\kappa\rho(\mathbf{x})\left[I_\theta(\mathbf{x}) - \int_0^{2\pi} p(\theta'\rightarrow\theta)\, I_{\theta'}(\mathbf{x})\, d\theta' \right] \tag{1}$$

where κ is the cross-section per particle, or unit of mass, depending on the choice of units for density ρ. Notice that the phase function $p(\theta'\rightarrow\theta)$ which has units of inverse radians and is not immediately assumed to be axisymmetric (dependent on $|\theta'\rightarrow\theta|$).

The usual strategies –diffusion and higher spherical harmonics– start by averaging eq. (1) and the phase function in direction space, hence the eventual introduction of angular "quadrature" where the (pivot) angles and their associated weights are far from arbitrary. By contrast, our approach starts by sampling direction space: let $\{\mathbf{i}\}$ be a finite but otherwise arbitrary set of directions. We now simply require the radiance field and phase function be decomposable into sums of δ-functions supported by $\{\mathbf{i}\}$:

$$I_{\mathbf{u}}(\mathbf{x}) = \sum_{\{\mathbf{i}\}} I_{\mathbf{i}}(\mathbf{x})\, \delta(\mathbf{u}-\mathbf{i}), \qquad p(\mathbf{j}\rightarrow\mathbf{u}) = \sum_{\{\mathbf{i}\}} P_{\mathbf{ji}}\, \delta(\mathbf{u}-\mathbf{i}),\ \mathbf{j}\in\{\mathbf{i}\}. \tag{2a,b}$$

Note that DA "radiances" $I_{\mathbf{i}}$ have units of flux (irradiance) and that the coefficients $P_{\mathbf{ij}}$ can be viewed as the elements of a (dimensionless) scattering matrix $\boldsymbol{P} = \{P_{\mathbf{ij}}\}$. Substitution of eqs. (2a,b) into the transfer equation (1) followed by $\mathbf{u}$-integration yields

$$\mathbf{j}\cdot\nabla I_{\mathbf{j}} = -\kappa\rho(\mathbf{x}) \sum_{\{\mathbf{i}\}} (1-P)_{\mathbf{ij}}\, I_{\mathbf{i}}(\mathbf{x}), \tag{3}$$

i.e., the DA radiative transfer equation –a finite (rather than infinite) system of coupled 1st order partial differential equations. As we will soon see, this particular phase function choice can be made in such a way that considerable conceptual and computational short-cuts become available. Naturally, the most useful 2-D DA phase functions depend only on relative angles (equivalently, $\mathbf{i}\cdot\mathbf{j}$) and this requirement in fact reduces[1] the number of possible choices for $\{\mathbf{i}\}$ to a countable infinity; this number is reduced to 2 if one is contemplating finite difference solution procedures since these call for a tessellation of the plane, a symmetry which the DA phase function must respect. (In d = 3, there are only five relative angle DA phase functions, each being associated with a Platonic solid –two of which can be retained for space-filling applications.) Most importantly, it has been shown numerically[3] on several examples that this drastic simplification of the angular part of the transfer does generally not affect the exponents such as ν_T discussed in section 1; analytical renormalization[2]- and similarity[1]-based arguments for this apparently very general phase function insensitivity in radiative scaling behavior have also be made.

2.2. Eigenanalysis of the orthogonal DA extinction/scattering matrix in two dimensions

We now place ourselves explicitly in d = 2: $\mathbf{x} = (y,z)^T$ where subscript "T" means transpose. This is obviously the minimal dimensionality where horizontal fluxes –the primary focus of this study– exist and, apart from easing the computational load, allows straightforward visualization of the full radiance fields. Furthermore, we take $\{\mathbf{i}\} = \{\pm\hat{\mathbf{y}},\pm\hat{\mathbf{z}}\}$, the unit vectors that orient the axii of the rectangular coordinate system along with their opposites. This is of course one of the DA systems associated with

plane-filling cells, namely, squares (a fact that we will be quick to exploit numerically in §4.3). The general DA transfer equation (3) then reads

$$\left[A_y \frac{\partial}{\partial y} + A_z \frac{\partial}{\partial z} \right] \mathbf{I}(\mathbf{x}) = \kappa\rho(\mathbf{x}) \, (\boldsymbol{P\text{-}1}) \, \mathbf{I}(\mathbf{x}) \tag{4}$$

where

$$\mathbf{I} = \begin{pmatrix} I_{+y} \\ I_{-y} \\ I_{+z} \\ I_{-z} \end{pmatrix}, \qquad A_y = \begin{pmatrix} 1 & 0 & 0 & 0 \\ 0 & -1 & 0 & 0 \\ 0 & 0 & 0 & 0 \\ 0 & 0 & 0 & 0 \end{pmatrix}, \qquad A_z = \begin{pmatrix} 0 & 0 & 0 & 0 \\ 0 & 0 & 0 & 0 \\ 0 & 0 & 1 & 0 \\ 0 & 0 & 0 & -1 \end{pmatrix}, \qquad \boldsymbol{P\text{-}1} = \begin{pmatrix} t\text{-}1 & r & s & s \\ r & t\text{-}1 & s & s \\ s & s & t\text{-}1 & r \\ s & s & r & t\text{-}1 \end{pmatrix}. \tag{5}$$

By inspection, we see that t, r and s are the probabilities (P_{ij}) of scattering through 0, π and $\pm\pi/2$ radians respectively. The d = 3 incarnations of eqs. (4)–(5) with different notations have been used previously[12] –and independently[13]– in various contexts. Introducing the following definitions

$$a = 1 - t - r - 2s, \qquad q = 1 - t + r, \qquad p = 1 - t - r, \tag{6}$$

we see that the relative weights of the P_{ij} in (6) are $(\mathbf{i}\cdot\mathbf{j})^n$ with n = 0, 1, 2 respectively. The above are therefore simply related to the 0^{th} through 2^{nd} coefficients of the Fourier series –or 2-D spherical harmonics– expansion of the DA phase function. In particular, we have $a = 1-\varpi_0$ and $q = 1-\varpi_0 g$ where ϖ_0 is the usual single-scattering albedo (or total probability of scattering). Excluding multiplying media where $a < 0$ ($\varpi_0 > 1$), the P_{ij} must all be less than one, we therefore necessarily have

$$0 \le a \le 1, \qquad 0 \le q \le 2, \qquad a \le p \le 1. \tag{7}$$

Equalities are obtained respectively for all/no scattering, all forward/backward scattering, and no/all side scattering.

Just as $1-\varpi_0$ and $1-\varpi_0 g$ are the first harmonics of the fundamental scattering-extinction kernel $\delta(\mathbf{u}'-\mathbf{u})-p(\mathbf{u}'\cdot\mathbf{u})$ that appears implicitly in the continuous angle transfer eq. (1), we find the following eigenvalues and -vectors for the scattering-extinction matrix ***P-1*** in (5):

$$a, \begin{pmatrix} 1 \\ 1 \\ 1 \\ 1 \end{pmatrix}, \qquad q, \begin{pmatrix} 0 \\ 0 \\ 1 \\ -1 \end{pmatrix} \text{and} \begin{pmatrix} 1 \\ -1 \\ 0 \\ 0 \end{pmatrix}, \qquad 2p\text{-}a, \begin{pmatrix} -1 \\ -1 \\ 1 \\ 1 \end{pmatrix}. \tag{8}$$

As in the continuous angle formulation, this type of decomposition is particularly useful in local similarity analysis:[14] the solutions of (4) are clearly left unchanged if the products κa, κq, and κp are all left unchanged. (Without loss of generality, we use a given constant $\rho(\mathbf{x})$ field and modulate only the optical parameters, so changes in optical thickness are via κ alone.) In particular, we see that the important class of conservative (a = 0) phase functions is invariant under similarity; furthermore, we find a = q = p = 0 (conservative all forward scattering) as the only –and trivial– fixed point of the similarity transformation.

Letting $I_{i\pm} = I_{+\mathbf{i}} \pm I_{-\mathbf{i}}$ ($\mathbf{i}=\hat{\mathbf{y}},\hat{\mathbf{z}}$), the projections of the (formal) radiance 4-vector **I** on the above three eigenspaces are respectively:

$$J = I_{y+} + I_{z+}, \qquad \mathbf{F} = \hat{\mathbf{y}} I_{y-} + \hat{\mathbf{z}} I_{z-}, \qquad X = - I_{y+} + I_{z+}, \tag{9}$$

i.e., total radiance (or scalar flux), net flux (2-vector), and (scalar) excess of vertically to horizontally propagating radiation.

2.3. Second order formulation and the singular diffusion limits in the conservative case

The above definitions can be used to obtain a more symmetric formulation of orthogonal DA transfer at 2^{nd} order in the directional derivatives. First, define a non-dimensionalized and rescaled gradient operator,

$$\nabla^\dagger = \frac{1}{q\kappa\rho(\mathbf{x})} \nabla = \begin{pmatrix} \delta_y \\ \delta_z \end{pmatrix}, \tag{10}$$

and the 2-vector $\mathbf{I}_+ = (I_{y+}, I_{z+})^T$. Starting from (4), a little algebra yields

$$\mathbf{F} = - \nabla^\dagger \mathbf{I}_+ \tag{11}$$

with, in the important case of conservative (a = 0) scattering,

$$\left[1 - \frac{q}{p} \delta_i^2 \right] I_{i+} = J - I_{i+} \quad (i=y,z) \tag{12a}$$

equivalently,

$$\left[\delta_y^2 + \delta_z^2 \right] J = - \left[\delta_y^2 - \delta_z^2 \right] X , \qquad \left[\delta_y^2 + \delta_z^2 - 4 \frac{p}{q} \right] X = - \left[\delta_y^2 - \delta_z^2 \right] J . \tag{12b,c}$$

We see that the l.h. sides contain the (inhomogeneous) diffusion operator since $\nabla^{\dagger 2} = \delta_z^2 + \delta_y^2 \propto \nabla \cdot D(\mathbf{x}) \nabla$ where $D(\mathbf{x}) = (2q\kappa\rho(\mathbf{x}))^{-1}$ is radiative diffusivity. With this choice, (11) reads exactly as Fick's law $\mathbf{F} = -D\nabla J$ as soon as X = 0 since this implies that $I_{z+} = I_{y+} = J/2$. Moreover, (12b) X = 0 reduces to the diffusion equation $\nabla \cdot D(\mathbf{x}) \nabla J = 0$; thus X will be called the "non-diffusive" component (of the DA radiance distribution).

Notice that the only phase function parameter left in eqs. (12a) or (12b,c) is the ratio q/p, which is invariant under similarity, and a similarity transformation leaves the solutions unchanged (by definition), the asymptotic scaling exponents discussed in section 1 are therefore the same for similar phase functions. This gives credence to the generally observed and much stronger phase function independence of the radiative exponents (which can be proven rigorously[1] for all DA phase functions within the context of a global DA similarity theory but with somewhat non-standard BCs). By way of contrast, we also notice that the (physically allowable) limit $p \to 0$ (vanishing side scattering) in eq. (12a) leads to decoupled 1-D diffusion equations in both y- and z-directions: we retrieve the IP approximation and (at constant $q > 0$) it is singular with respect to the similarity relations so we do not expect the same exponents to arise in general. The more interesting 2-D diffusion approximation is obtained[15] by taking the (unphysical) limit $p \to \infty$ in eq. (12c). This can be done by simultaneously requiring a vanishing projection on the corresponding eigenvector (i.e., X = 0); we notice that this previously[61] uncharted route from transfer to diffusion leaves the latter's similarity theory[62] untouched as it should (specifically, we require $\kappa q \propto (1-g)\tau$ = const. from Fick's law in conservative systems). Of course, this limit is also singular (at constant $q < \infty$) and diffusive approximation exponents will generally differ from their exact transfer counterparts. An example of this strikingly different behavior between diffusive and kinetic transport is provided by random binary mixtures of full and empty cells at "percolation" threshold[1,16] (when an infinite cluster of empty cells appears: e.g., 59.28% empty for square lattices in d = 2).

3. RANDOM MULTIPLICATIVE CASCADE PROCESSES - BASIC IDEAS WITH EXAMPLES

Soon after the publication of Kolmogorov's landmark "1941" paper[17] on the scaling properties of turbulence in the inertial range, his assumption of spatial uniformity of the rate of dissipation of kinetic energy ($\varepsilon = \partial v^2/\partial t$) came under attack.[18] In the early '60s, two competing models emerged to account for the high degree of intermittancy ("spottiness") observed in fully developed turbulence: the log-normal model[19,20] which is the prototypical "multifractal," on the one hand, and the model of pulses-within-pulses[21] which turns out to be a good exemple of a "(mono)fractal," on the other hand. (Of course, the terms "fractal" and "multifractal" were coined in the mid-'70s and -'80s respectively.[22,23]) Both models build on Richardson's simple idea of a turbulent "cascade" where the nonlinear terms that dominate the dynamics in the inertial range are responsible for breaking up larger "eddies" into ever smaller ones.[24] The two basic options are illustrated in Figs. 1–2 where we see such a process developing in d = 2 with the daughter eddies, becoming either "dead" (for once and for all) or remaining "alive" (for the moment) or simply "weaker" or "stronger." Both illustrated examples use a "discrete" cascade (for commodity), i.e., the scale dividing ratio is $\lambda_0 = 2$; after n steps, the total range of scales is $\lambda = \lambda_0^n$. Letting $\mu\varepsilon_i$ be the i^{th} multiplicative increment of the dissipation field at some point on the d-dimensional grid, we find

$$\varepsilon_n = \varepsilon_\lambda = \varepsilon_0 \prod_1^n \mu\varepsilon_i \qquad \ln\left(\frac{\varepsilon_\lambda}{\varepsilon_0}\right) = \sum_1^n \ln(\mu\varepsilon_i) \tag{13a,b}$$

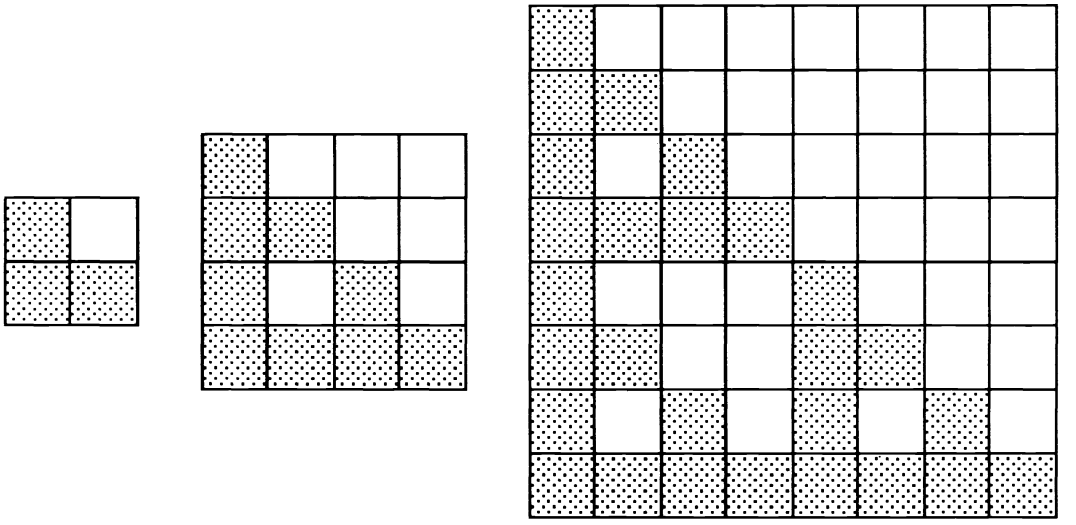

Fig. 1: Generation of a deterministic monofractal cloud in d = 2 spatial dimensions (first three steps, at constant inner scale l_0) with $D = \log_2 3 = 1.585\cdots$.

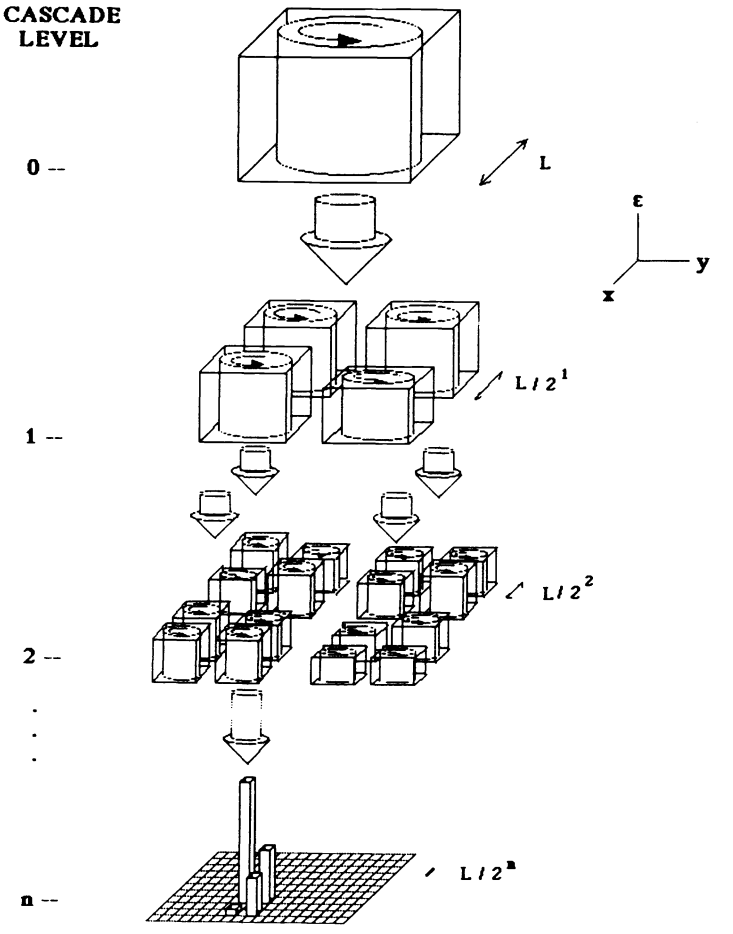

Fig. 2: Generation of a random multifractal cascade field in d = 2 spatial dimensions (schematic, at constant outer scale L).

for the n^{th} iterate of (the appropriately non-dimensionalized) ε. One can take $\varepsilon_0 = 1$ without loss of generality, especially in the present context of stochastic optical media (because of the remaining free parameter κ).

The random version of the fractal illustrated in Fig. 1 is the so-called "β" model and corresponds to the following (Bernouilli) law with two parameters which are constrained by a (turbulent cascade flux) conservation relation:

$$\mu\varepsilon = \begin{cases} \lambda_0^{\gamma_+} & \text{Prob} = \lambda_0^{-C} \\ 0 & \text{Prob} = 1-\lambda_0^{-C} \end{cases} \qquad \text{with} \quad \log_{\lambda_0}\langle\mu\varepsilon\rangle = \gamma_+ - C = 0, \tag{14}$$

where "conservation" means that we will have $\langle\varepsilon_\lambda\rangle = 1$ at all steps in the cascade since the $\mu\varepsilon_i$ are chosen independently but not at every realization; i.e., this conservation is not exact (as in radiative transfer) but rather a statistical property. C is the "codimension" of the limiting ($n\to\infty$) fractal set; notice that $C \geq 0$, with homogeneity retrieved at equality. The number of cells still "alive" (at the $\lambda_0^{n\gamma_+}$ activity level) after n steps is $(\lambda_0^d)^n(\lambda_0^{-C})^n = \lambda^{d-C} \ll \lambda^d$ (the total number of cells on the grid) as soon as $C > 0$ and $\lambda \gg 1$. We are indeed dealing with a very sparse set, and $D = d-C$ is its "fractal" dimension that replaces d, the dimensionality of space, in the fundamental mass/size relation:

$$N_{1/\lambda}(\varepsilon_\lambda > 0) \sim \lambda^D \tag{15}$$

for the number of ($1/\lambda$-sized) active cells. The log-normal model is also defined by two parameters (and a conservation constraint between them):

$$\mu\varepsilon = e^\Gamma, \quad dP(\Gamma) = \frac{1}{\sqrt{2\pi}}\, e^{-\frac{(\Gamma-m)^2}{2\sigma^2}} \frac{d\Gamma}{\sigma} \qquad \text{with} \quad \ln\langle\mu\varepsilon\rangle = \tfrac{1}{2}\sigma^2 + m = 0. \tag{16}$$

We need the probability density function (p.d.f.) for the ε_λ field variables too. First, define the "order of singularity" of the n^{th} generation dissipation field, i.e., at a some resolution $1/\lambda = \lambda_0^{-n}$ (to 1):

$$\gamma = \log_\lambda(\varepsilon_\lambda), \tag{17}$$

then

$$\text{Prob}(\lambda^\gamma \leq \varepsilon_\lambda < \lambda^{\gamma+d\gamma}) = \lambda^{-c(\gamma)}\, d\gamma \tag{18}$$

provides a natural scaling parameterization. $c(\gamma)$ is called the "codimension function" since it determines the fractal dimension of the exceedence sets of the ε_λ field for any given threshold λ^γ. To see this, recall that the ε-field has been generated down to resolution $1/\lambda$ on a d-dimensional grid with λ boxes on a side; the number of boxes required to cover an exceedence set is therefore:

$$N_{1/\lambda}(\varepsilon_\lambda \geq \lambda^\gamma) = \lambda^d\, \text{Prob}(\varepsilon_\lambda \geq \lambda^\gamma) = \lambda^d \int_\gamma^\infty \lambda^{-c(\gamma')}\, d\gamma' \sim \lambda^{d-c(\gamma)} \tag{19}$$

where the "~" relation is introduced to absorb both prefactors (e.g., $c'(\gamma)$) and slowly varying scale dependent terms (e.g., $\ln\lambda$). Using eq. (19), it can also see that, in our notation, the fractal dimension $d-c(\gamma)$ –when positive– corresponds to the "$f(\alpha)$" used by many authors, mainly involved in strange attractor studies[25] with their "α" being equated to our $d-\gamma$ since, in that context, focus is on the "measure" $\varepsilon_\lambda\lambda^d$ itself –rather than its "density" ε_λ– as a function of the size of the averaging set ($1/\lambda$) –rather than λ. As in section 2 on radiative transfer, our multifractal notation is independent of d; this is an important advantage in stochastic modelling since the very large sample-space can be formally related[26] to the limit $d\to\infty$.

The $c(\gamma)$ for the log-normal model in eqs. (16) is readily obtained by using the well-known properties of sums of n independent Gaussian deviates of identical (m,σ) –namely, $m \to nm$ and $\sigma^2 \to n\sigma^2$– while the definitions (17)–(18) dictate the change of variable $\Sigma_i\Gamma_i \to n(\ln\lambda_0)\gamma$; hence, collecting results, we obtain

$$c(\gamma) = \frac{\ln\lambda_0}{2\sigma^2}\left(\gamma - \frac{m}{\ln\lambda_0}\right)^2 \qquad c(\gamma) = \frac{C_1}{4}\left[\frac{\gamma}{C_1} + 1\right]^2 \tag{20a,b}$$

where, in (20b), we have changed the parameterization to $C_1 = \sigma^2/2\ln\lambda_0 = -m/\ln\lambda_0$, as justified below and incorporating the conservation rule. Notice that, in the above, we have dropped the normalization constant $-\log_\lambda[\sqrt{\ln\lambda/2\pi\sigma^2}] = \log_{\lambda_0}[4\pi C_1/n]/n$ which is $\sim O(\log n/n)$ for large n –except if C_1 is vanishingly small. The lognormal cascade model therefore generates a whole family of fractals, each with its codimension: it is a multifractal. By contrast, comparing (15) with D = d-C and (19), we see that the simple fractal model (14) has

$$c(\gamma) = \begin{cases} 0 & \text{for } \gamma = -\infty \text{ (an almost sure event)} \\ C & \text{for } -\infty < \gamma \leq \gamma_+ \\ \infty & \text{for } \gamma > \gamma_+ \text{ (an impossible event)} \end{cases} \tag{21}$$

Having a single fractal dimension in its spectrum, it is best called a monofractal. In order to obtain a $c(\gamma)$ directly comparable to that of the log-normal multifractal, we must use (18) rather than (19); this yields a "defective" (sub-normalized) p.d.f. entirely concentrated at $\gamma = \gamma_+$ with a complementary "peak" placed (formally) at $\gamma = -\infty$.

Mathematically speaking, monofractals are defined by ("measure" zero) sets, hence they are purely geometrical in nature, whereas multifractals are defined in the (weak) limit of singular measures, hence the $c(\gamma)$ are fundamentally statistical exponents (although they can often be given a geometrical interpretation). Since it has been shown[27,28] that multifractality is obtained merely by changing the event $\mu\varepsilon = 0$ to $\mu\varepsilon = \lambda_0^{\gamma_-}$ ($\gamma_- > -\infty$) in (14), monofractals are clearly a very restricted class of models unlikely to occur in Nature. From the cloud modelling point of view, multifractals provide *bone fide* optical density fields, potentially extremely variable, whereas monofractals are made up of random conglomerations of homogeneous, cloudy cells separated by optical voids of all sizes. It is clearly of interest to find a family of gradually more multifractal models that provide a valid interpolation between monofractals and log-normal multifractals. "Universal" multifractals[29] do just this; moreover, they contain a representative example of the more interesting entries in a recently[30] proposed general classification of multifractal behavior and, finally, their parameters have been fitted to very diverse geophysical signals using various statistical techniques.[26,31]

4. RANDOM MULTIFRACTAL OPTICAL MEDIA - A CASE STUDY

4.1. The rationales for the statistical parameters of the adopted nominal density field

In order to obtain an unambiguous illustration of the radiative effects of scaling inhomogeneity, we require our model optical density field to exhibit (i) a large range of scales, (ii) a large range of values, (iii) well-understood mathematical properties and (iv) some degree of physical justification. The lognormal multifractal model described in section 3 automatically fulfills requirements (i), (ii) and (iii) as soon as λ (equivalently, n) and C_1 are given reasonably large values, say:

$$\boxed{\lambda = 2^n = 1024} \text{ and } \boxed{C_1 = 0.5} \tag{22}$$

The latter value is in the range one finds using the intermittancy corrections quoted in the literature needed to account for the discrepancy between -5/3 and observed power spectra of turbulent velocity. We have of course chosen $\lambda_0 = 2$, for commodity. A choice of $C_1 > 1$ would have made the intermittancy such that 1-D transections would meet vanishingly small amounts of material (fractal intersection theorem[60]); this would be a natural choice for modelling a sparse ("broken") cloud field with accordingly little scattering on average whereas, here, we are interested in optically thick media dominated by multiple scattering – a single massive cloud. The deep connections of multifractals with turbulence –the primary source of inhomogeneity in clouds– are now well established and they have completely superseded the monofractal models used justifiably (for simplicity) in our previous radiative studies. Still, item (iii) deserves a more detailed discussion. Dissipation ε is not density ρ; in particular, the spectral exponent of ε lies above -1 whereas that of ρ is observed to be close to -5/3. Although methods applicable to the concentration of scalars passively advected by fully developed turbulence –based on phenomenology[32,33]– are actively being researched,[29,34] no completely satisfactory stochastic model for the fluctuations of ρ has yet been devised; so criterion (iii) takes precedence and we make the somewhat extreme assumption that ρ (general, in section 2) = ε (log-normal, in section 3) with the parameters stated in (22).

Figs. 3a,a' show respectively the specific realization in order of singularity representation (i.e., $\gamma(\mathbf{x}) = \log_{1024}(\rho(\mathbf{x}))$, with linear palette) and the portion of its theoretical scale invariant histogram pertaining to a single realization, with remarkable values highlighted, i.e., $c(\gamma) \leq d = 2$. Notice the well distributed (space-filling) shade of grey corresponding to the theoretically most

Figs. 3. $C_1 = 0.5$ lognormal multifractal density field in d = 2 after n = 10 cascade steps (see text for details):

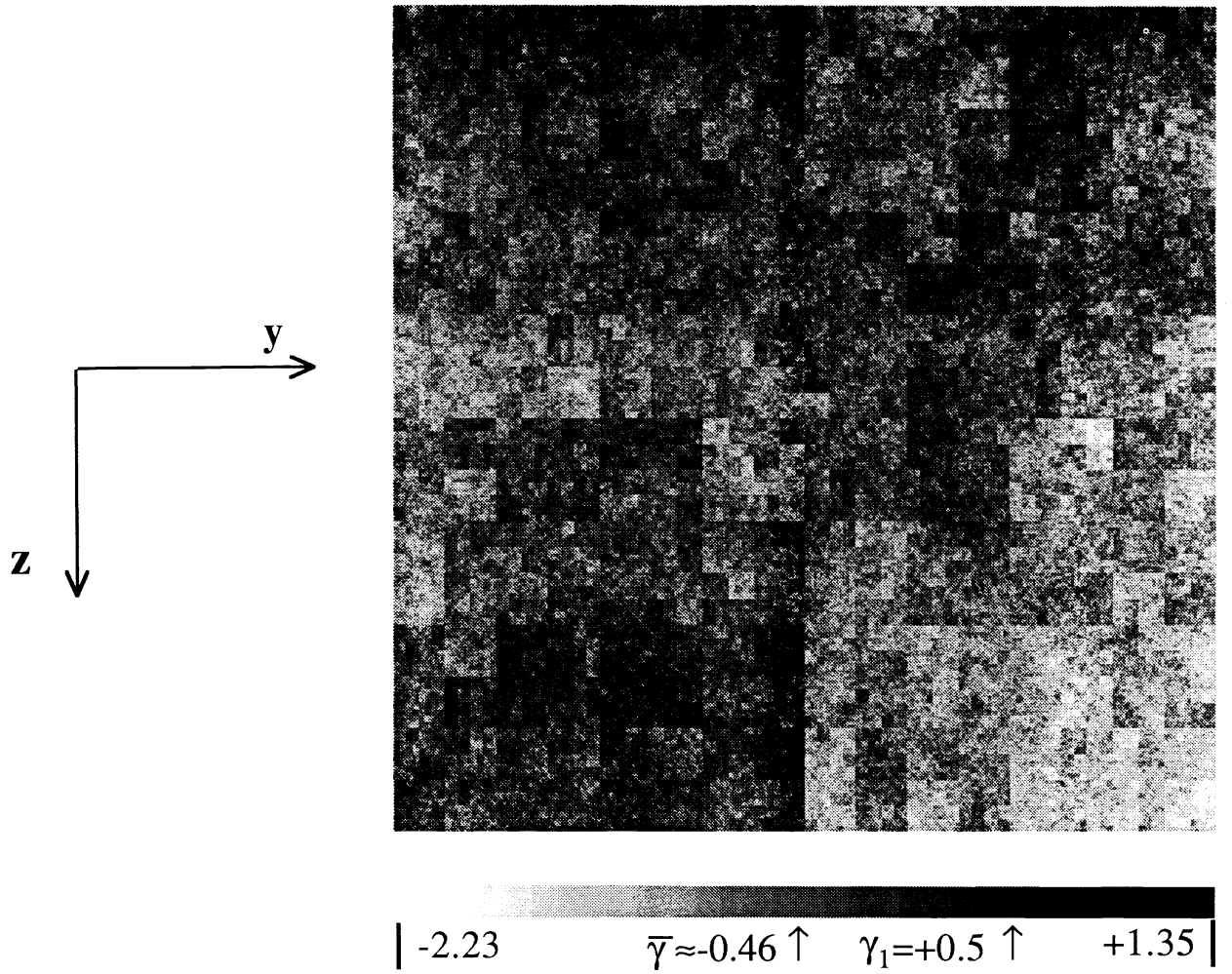

(a) grey scale map of the singularities,

Theoretical codimension function for singularities well-sampled in only one large 2-D realization:

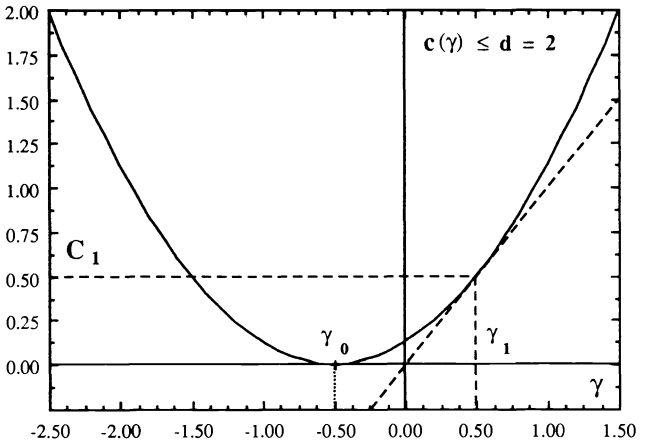

(a') c(γ) function.

Figs. 3. Cont'd:

(b) column-averaged densities and associated singularities,

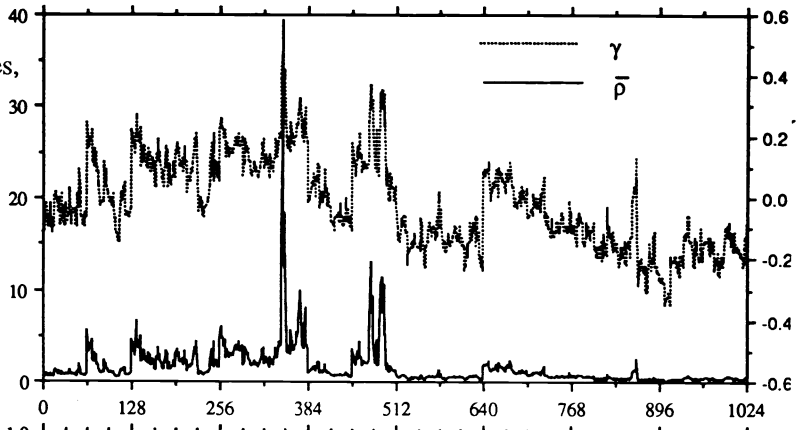

(b') independent pixel responses
(direct and total transmittances).

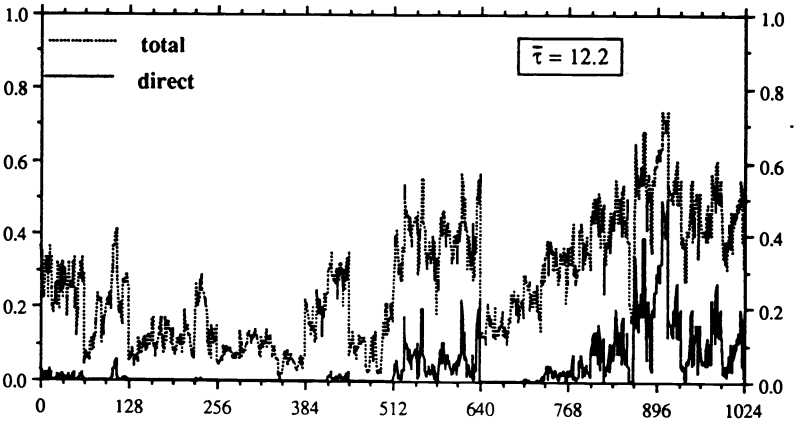

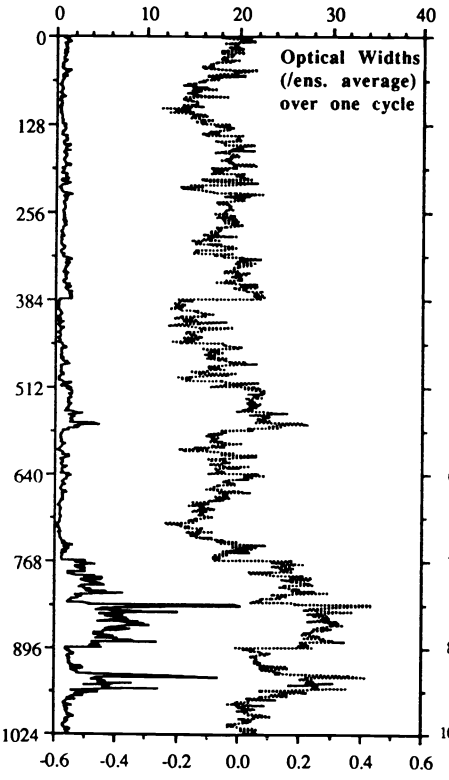

(c) row-averaged densities and associated singularities,

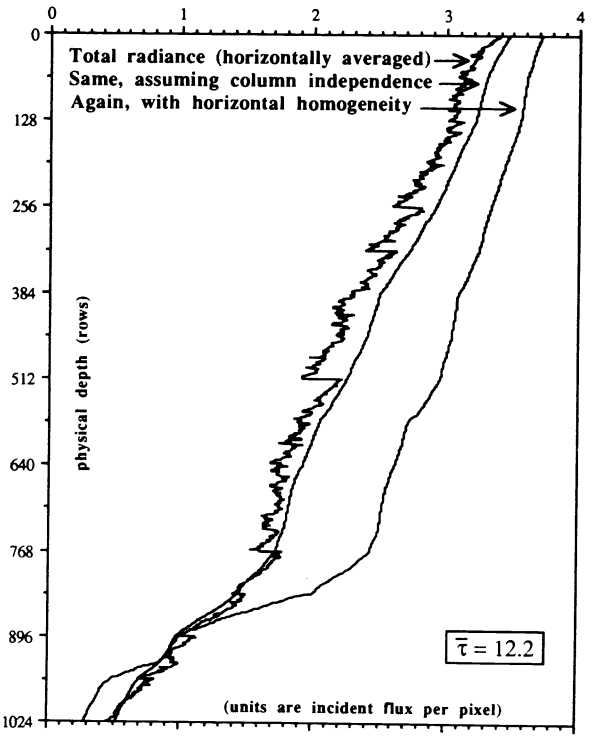

(c') row-averaged internal fields of total radiance
(homogeneous layers, independent pixels, numerical solution).

probable singularity $\gamma_0 = -C_1 = -0.5$ which has $c(\gamma_0) = 0$ and is very close to our example's $\overline{\gamma} \approx -0.46$. We have also singled out the point where $c(\gamma) = C_1$. The (positive) solution, γ_1, of this equation can be shown to be the order of singularity that is generically associated with the mean of the process, $\langle\varepsilon_\lambda\rangle$. It has the remarkable property of being where the $c(\gamma)$ curve is tangent to the first diagonal (i.e., $c'(\gamma_1) = 1$ and $\gamma_1 = C_1$) whether the multifractal is log-normal or not. In turn, this general property of (conserved) cascades can be used to define C_1 for any multifractal; C_1 therefore provides a convenient measure of the "mean" inhomogeneity.

To further emphasize the degree of concentration in the lower l.h. side of the medium, we have plotted the column-averaged densities and associated orders of singularity in Fig. 3b, i.e.,

$$\overline{\rho}_y = \frac{1}{L}\int_0^L \rho(y,z)\, dz, \qquad \gamma_{\overline{\rho}}(y) = \log_\lambda(\overline{\rho}_y), \tag{23}$$

and similarly for (row-averaged) $\overline{\rho}_z$ in Fig. 3c. The overall spatial average of this realization is $\overline{\rho} \approx 1.52$ which is not a rare fluctuation from the ensemble average $\langle\rho\rangle = 1$; these stochastic systems are stationary by construction. The individual ρ-values span a range from $\approx 10^{-7}$ to $\approx 10^4$. This can be compared with a fluctuation ratio of $\approx \lambda^{4\sqrt{dC_1}} \approx 10^{12}$ which is predicted from eq. (20b) and the above criterion[26] (namely, $c(\gamma) \le d$). While these huge fluctuations occur over the whole cloud, ≈2–4 ratios will not be rare from one pixel to the next since we must use $\sigma = \sqrt{2\ln 2 C_1} = 0.833\cdots$ in eqs. (16). Letting $\tilde{}$ denote the Fourier transform and $\mathbf{k}$ the wave vector, we find in the isotropic power spectrum of $\rho(\mathbf{x})$,

$$E_\rho(k) = \int_{|\mathbf{k}'|=k} \langle|\tilde{\rho}(\mathbf{k}')|^2\rangle\, d^2\mathbf{k}' = \int_0^{2\pi} \langle|\tilde{\rho}(k\mathbf{u}(\theta))|^2\rangle\, d\theta \tag{24}$$

a spatial/ensemble statistic which generalizes the spatial and/or ensemble mean since $\overline{\rho} = \tilde{\rho}(\mathbf{0})$ for every realization. As mentioned above, theory[35] predicts the spectrum of ε (hence our current hypothesis for ρ), $E_\rho(k)$, to scale as k^{-1+2C_1} (in our notations); hence in our particular case and $E_\rho(k)$ is independent of k. By contrast, 2-D uncorrelated (white) noise has a constant spectral "density" $E_\rho(k)/k^{d-1}$ hence $E_\rho(k) \sim k$ in d = 2; such media have been investigated both numerically[36] and analytically[37,38] (as a limit of exponentially decorrelating media) and are found to have quasi-homogeneous behavior, unsurprisingly in view of the lack of long range correlations that are built into multifractals as well as their even more characteristic intermittancy.

4.2. The optical parameters, albedo problem boundary conditions and independent pixel responses

The only physical parameters left to specify are purely optical: t, r, s, and κ. We can view the latter as an arbitrary overall numerical multiplier of the raw density field that converts it to "optical density" or "extinction coefficient." For practical (numerical) purposes, we want the medium to be optically thin at this homogeneity (pixel, l_0) scale –at least, on average– hence $\kappa\overline{\rho}l_0 \approx \kappa l_0 \ll 1$. At the same time, we want a large overall optical thicknesses (as required in "cloud"): $\kappa\overline{\rho}L \approx \kappa\lambda l_0 \gg 1$. When $\lambda = L/l_0 = 2^{10}$, these constraints are both fulfilled if κ is kept in the range 2^{-7}–2^{-3} in natural units (where $l_0 = 1$). So, apart from constants, Fig. 3b illustrates

$$\tau_y = \int_0^L \kappa\rho(y,z)\, dz = \kappa\,\overline{\rho}_y\, L; \qquad \overline{\tau}_\lambda = \frac{1}{L}\int_0^L \tau_y\, dy = \kappa\,\overline{\rho}\,L \tag{25a,b}$$

being total optical thickness. Taking κ as a negative integer power of 2, we are left with 5 optical media, all commensurate with our nominal log-normal cascade field; their total (or spatially averaged) optical thicknesses $\overline{\tau}_\lambda$ being in the range 12.2–195. We will dwell mainly on the extremes in the remainder of this paper. For (numerical and conceptual) simplicity, we assume conservative isotropic DA scattering (t = r = s = 1/4 hence a = 0, q = 1, p = 1/2) but our results are somewhat more general since, by similarity, any DA phase function with q/p = 2 will yield the same results, but at different κ's.

As presented in section 2, transfer theory relates the optical density and radiation fields in a purely local manner; BCs are required to determine the latter completely. In early investigations using both transfer[39] and diffusion[40] methods, horizontal radiative fluxes were induced simply by changing the support of the (otherwise homogeneous) optical medium from an infinite

slab to a finite cuboid. Since we now want to isolate variability-induced horizontal fluxes, (meteorologically) we think of our cloud as "extended" and (mathematically) we impose cyclical conditions in the horizontal direction –and simply "recycle" photons in the Monte Carlo scheme:

$$I_{\pm y}(0,z) = I_{\pm y}(L,z) \qquad (0 \le z \le L), \tag{26a}$$

in DA transfer. We are primarily interested in the (DA) problem of diffuse reflection and transmittance which is defined by the following vertical BCs:

$$I_{+z}(y,0) = 1, \quad I_{-z}(y,L) = 0 \qquad (0 \le y \le L). \tag{26b}$$

In many respects, the most important unknowns in this (so-called "albedo") problem are the exiting radiance fields which, in DA transfer, read as:

$$R(y) = I_{-z}(y,0), \quad T(y) = I_{+z}(y,L) \qquad (0 \le y \le L) \tag{27}$$

for local reflectance and transmittance respectively. At the lowest level of spatial resolution (as considered in our previous studies, discussed in section 1), the response of the inhomogeneous medium is of course defined by:

$$T = \frac{1}{L} \int_0^L T(y)\, dy = 1 - R \tag{28}$$

where the last step makes use of an obvious global consequence of the local conservative property we assumed for the DA phase function (a = 0). This hypothesis makes our calculations most readily comparable to radiative transfer in the visible part of the solar spectrum where the cloud-free atmosphere is quasi-transparent and (pure) liquid water has vanishingly small absorption; the most equivalent continuous angle illumination conditions would be overhead sun, or a uniform (at least axisymmetric) distribution of diffuse radiance.

In Fig. 3b', we have plotted the total (IP)- and direct transmittances of each column for the thinnest cloud, i.e., respectively

$$T_p(\tau_y) = \frac{1}{1 + r\tau_y}, \qquad T_d(\tau_y) = \exp[-\tau_y]. \tag{29a,b}$$

The former corresponds to the case of conservative (a = 0, $\varpi_0 = 1$) scattering in d=1 or with no side scattering (s = p = 0); we then have r = q/2 = (1-g)/2 so –as in any standard two-flux theory[58,59]– T_p is a universal function of rescaled optical thickness, (1-g)τ. $T_p(\tau)$ is also $1/(1+r\tau)$ for any conservative DA phase function but in the very restricted case of homogeneous plane-parallel media. The latter is the solution to the sourceless ($\varpi_0 = 0$) transfer problem: t = r = s = 0 hence a = q = p = 1. We notice that $T_d(\tau_y)$ can far exceed $T_d(\bar{\tau}) \approx 10^{-5.3}$ and its extreme intermittancy which is not too surprizing since our[10] analytical investigation into direct transmittance through multifractals shows it to have very simple (monofractal-like) scaling statistics in the limit $\lambda \to \infty$ and on condition that this corresponds to increasing optical thickness. In the same limit and conditions, $\langle T_p(\tau_\lambda)^h \rangle$ –with a multifractal τ_λ-distribution– is found[10] to scale like $\langle \tau_\lambda^{-h} \rangle$ for h>0 but not too large; the result being independent of r, we again find radiative exponents independent of phase functions. (The related Fig. 3c' is discussed in §4.4.)

4.3. The numerical procedures and validation

We must now settle on a numerical procedure to solve (4) with BCs (26a,b) and validate it. Given the novelty of the type of optical medium investigated (with its extreme variability being a particular concern), we have decided to use the most straightforward approach available: Monte Carlo simulation which can be considerably speeded up in DA transfer. Photons are tracked continuously in space and detected by digital counters at every pixel boundary crossing. The validity of the code was established by applying to our thinnest medium the next most straightforward approach available, namely, (Gauss-Seidel) relaxation of the finite difference equations obtained from (4) on a square lattice. During preliminary runs (at n = 5, λ = 32), it became apparent that decimating the (DA) radiation fields on a finer grid than the density field did not improve the accuracy significantly. Nor did it help (in terms of overall convergence time) to use the radiation fields associated with previous (n = 1,⋯,4) cascade steps; the optimal initialization strategy seems to be to use the analytically known solution for the internal radiation fields corresponding to the IP approximation. Specifically, we assume $\delta_y = 0$ hence (11) gives us $I_{y-,y}(z) = 0$, and (12) $I_{y+,y}(z) = I_{z+,y}(z)$; this last quantity is given by

$$I_{z+,y}(z) = I_{z+,y}(0) + \left(\frac{dI_{z+}}{d\tau'}\right)_y \tau'_y(z) \quad \text{with } I_{z+,y}(0) = 1+R(\tau_y), \quad \left(\frac{dI_{z+}}{d\tau'}\right)_y = -2R(\tau_y), \quad \text{and } \tau'_y(z) = \int_0^z \kappa\rho(y,z')\, dz' \qquad (30)$$

which verifies $\delta_z^2 I_{z+,y} = 0$ and where $R(\tau_y) = 1-T(\tau_y)$. We also have $I_{z-,y} = T_p(\tau_y)$ that can be computed from eq. (29a). Definitions finally yield the four required DA radiances: $I_{\pm z,y}(z) = [I_{z+,y}(z) \pm I_{z-,y}]/2$ and $I_{\pm y,y}(z) = I_{z+,y}(z)/2$. For roughly constant CPU time (several hours on a Cray 2), the relaxation technique yields results that are somewhat more accurate simply because they are not contaminated with the noise which is characteristic of Monte Carlo. As expected, the two methods agree to within this (Poissonian) noise level which, in the circumstances (10^3–10^4 photons injected per pixel), is at the 1-5% level for the internal/exiting fields and a few ‰ for the overall responses. Given that we haven't even considered ensemble-averages yet, the above brute force –and overkill– approach is unviable in the long run; eventually, we will require a combination of more CPU time, improved numerical methodology (e.g., sparse matrix rather than relaxation techniques) as well as a clearly defined statistics to target optimally, using Monte Carlo "double randomization"[41] if necessary. Other reasons to improve Monte Carlo algorithms in spite of the difficulty of accelerating them by vectorization are that (i) massively parallel supercomputers will soon become widely available and there is no limit to how many photons can be processed simultaneously in linear transfer problems, and that (ii) they have a natural by-product: the orders-of-scattering decompositions of the various flux fields (their utility is briefly discussed in the concluding section 5). For the present, the Monte Carlo method is retained for the thicker media simply because of its greater generality (one doesn't have to worry about increasingly thick cells somewhere in the medium). Finally, we note that the conceptual simplification of cyclical horizontal BCs does carry a computation time cost in both of the methods that we implemented.

4.4. The internal radiation vector fields in their eigenvector representations

In Figs. 4–7a ($\overline{\tau}$ = 12.2) and Figs. 4–7b ($\overline{\tau}$ = 195), we present grey scale renderings of the four eigenspace projections of the DA radiance fields as defined in eqs. (9): (Figs. 4) J, (Figs. 5) F_y, (Figs. 6) F_z, and (Figs. 7) X; this choice has proved more useful to us than the radiances themselves which will be made available elsewhere.[42] Grey scales are all linear in DA radiance (of which each pixel receives one unit) and we have indicated min's, max's and (Figs. 5–7) means. Before any further discussion, it is important to "see" the amount of information contained in these two plates; this is best done by mentally visualizing the results one would find for isotropic DA scattering in a totally homogeneous plane-parallel medium: (Figs. 4) a uniform linear decrease in J (hence picture the grey scale at the right stretched to the full frame-width of these figures, (Figs. 5) $F_y = 0$ (blank picture), (Figs. 6) $F_z = T(\overline{\tau})$ = const. (some uniform shade of grey), and (Figs. 7) X = 0, diffusion applies everywhere exactly (blank picture). The most casual glance at Figs. 4–7 is sufficient to see how severely this symmetry is broken by our example of internal variability but any amount will produce some perturbation by a mechanism that has been described[43] as a "mode-coupling" induced by a source/sink-like term that appears on the r.h.s. of the (usual, d=3, counterpart of) transfer eq. (1) after harmonic analysis in **u** and Fourier analysis in (x and) y, but not z. Equally striking is the fact that the 10^{11}-range variability of the ρ-field has been compressed into ranges ≈2 in J which is strictly positive and ranges of ≈2–4 for the maximum absolute values of the other (algebraically valued) quantities using, as point of comparison, $T = \overline{F_z}(y)$ which remains constant with respect to y (by conservation of total radiant energy flux). In other words, the radiation fields inside such a strongly and intermittently variable but single cloud are only weakly variable and it is unclear as to how one could find their "residual" intermittancy. This sharply contrasts with our knowledge of the exiting radiation from whole cloud (and surface reflectance) fields (see §4.5 for further discussion of this point). It is nevertheless very important to find –however subtle– the signature of all the relevant statistical features of $\rho(\mathbf{x})$ –including intermittancy– in the radiation field if we are ever going to develop (stochastically robust) inversion schemes for remotely-sensed data, i.e., finding the statistics of the ρ field from, say, those of the albedo field.

The most striking feature in Fig. 4a is the prominence of the rectangular grid structure which has, however, almost vanished from Fig. 4b; this provides a (first) illustration of the smoothing power of multiple scattering when boosted by an overall 16-fold increase in optical density. The artifact is of course due to the phótons' propagation being restricted to the axes of the grid which are also (artificially) enhanced by the "discrete" nature of the cascade, cf. the visually obvious grid lines in Fig. 3a. This is not an inherent limitation of the multifractal model since the software to generate "continuous" cascades exists[34] and we will not remain commited to DA transfer when efficient and reliable continuous angle inhomogeneous transfer code becomes available. (The authors will gladly communicate –digitally speaking– their $\rho(\mathbf{x})$-field to any worker in the field who wishes to experiment with it and compare results and/or performance.) For the moment, this "texture" is in fact useful for tracking visually the $\rho(\mathbf{x})$-$J(\mathbf{x})$ connections: notice the more pronounced gradients in the denser regions; these come in all sizes (hence strengths) but the foremost lie in the lower l.h.s. In Fig. 3c', we have plotted the results of three different ways of calculating the row-averaged

Figs. 4. Total DA radiance fields (J):

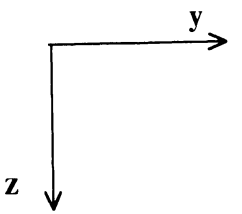

(a) $\overline{\tau}$ = 12.2 (or $\log_2\kappa$ = -7),

(b) $\overline{\tau}$ = 195 (or $\log_2\kappa$ = -3).

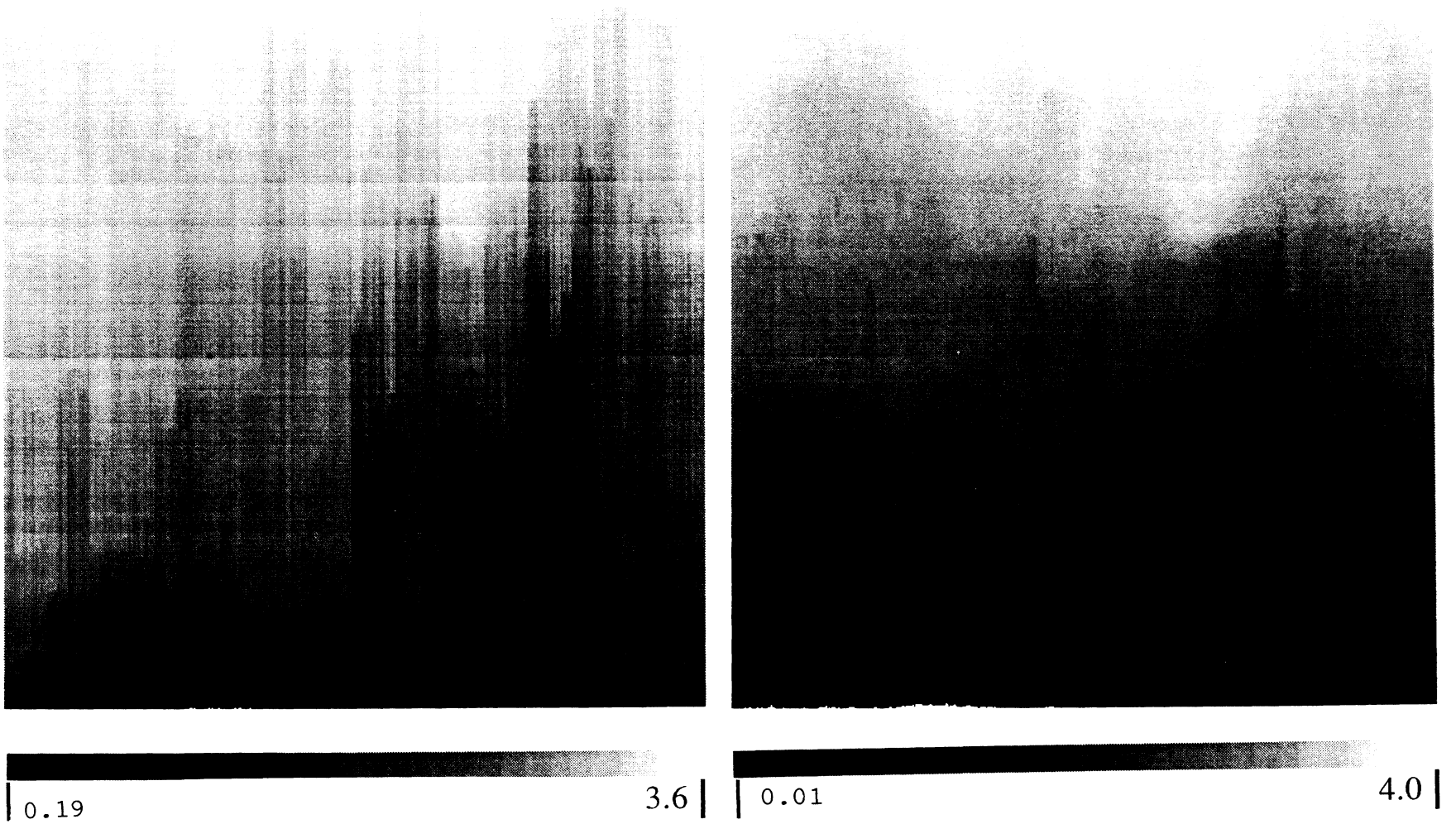

Figs. 5. Horizontal net flux component of DA radiance fields (F_y):

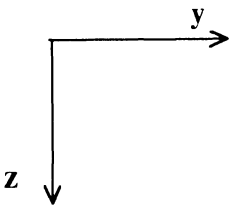

(a) $\overline{\tau}$ = 12.2 (or $\log_2\kappa$ = -7),

(b) $\overline{\tau}$ = 195 (or $\log_2\kappa$ = -3).

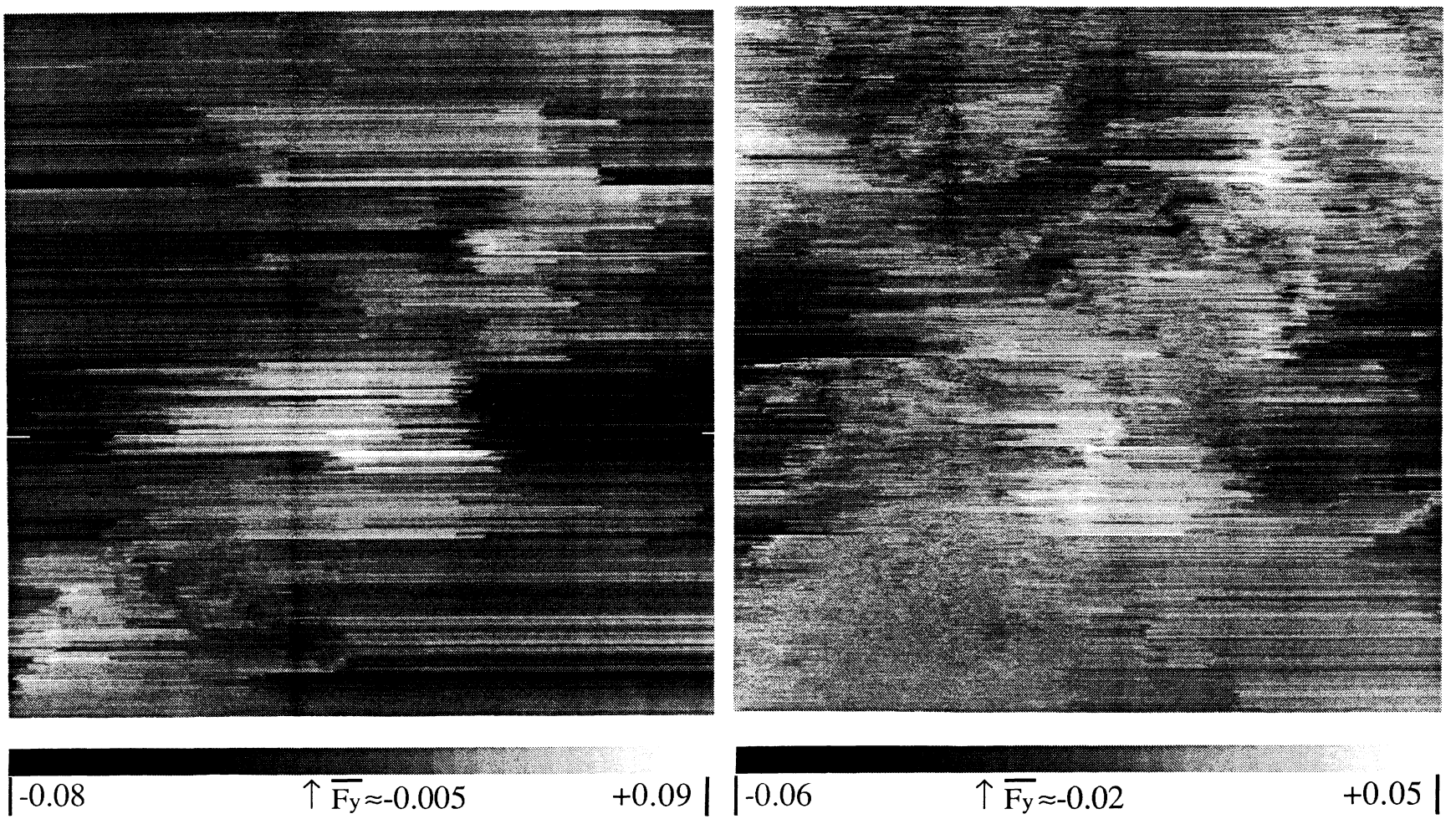

Figs. 6. Vertical net flux component of DA radiance fields (F_z):

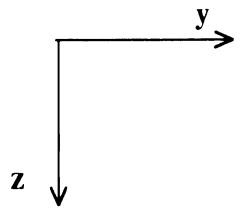

(a) $\overline{\tau}$ = 12.2 (or $\log_2\kappa$ = -7),

(b) $\overline{\tau}$ = 195 (or $\log_2\kappa$ = -3).

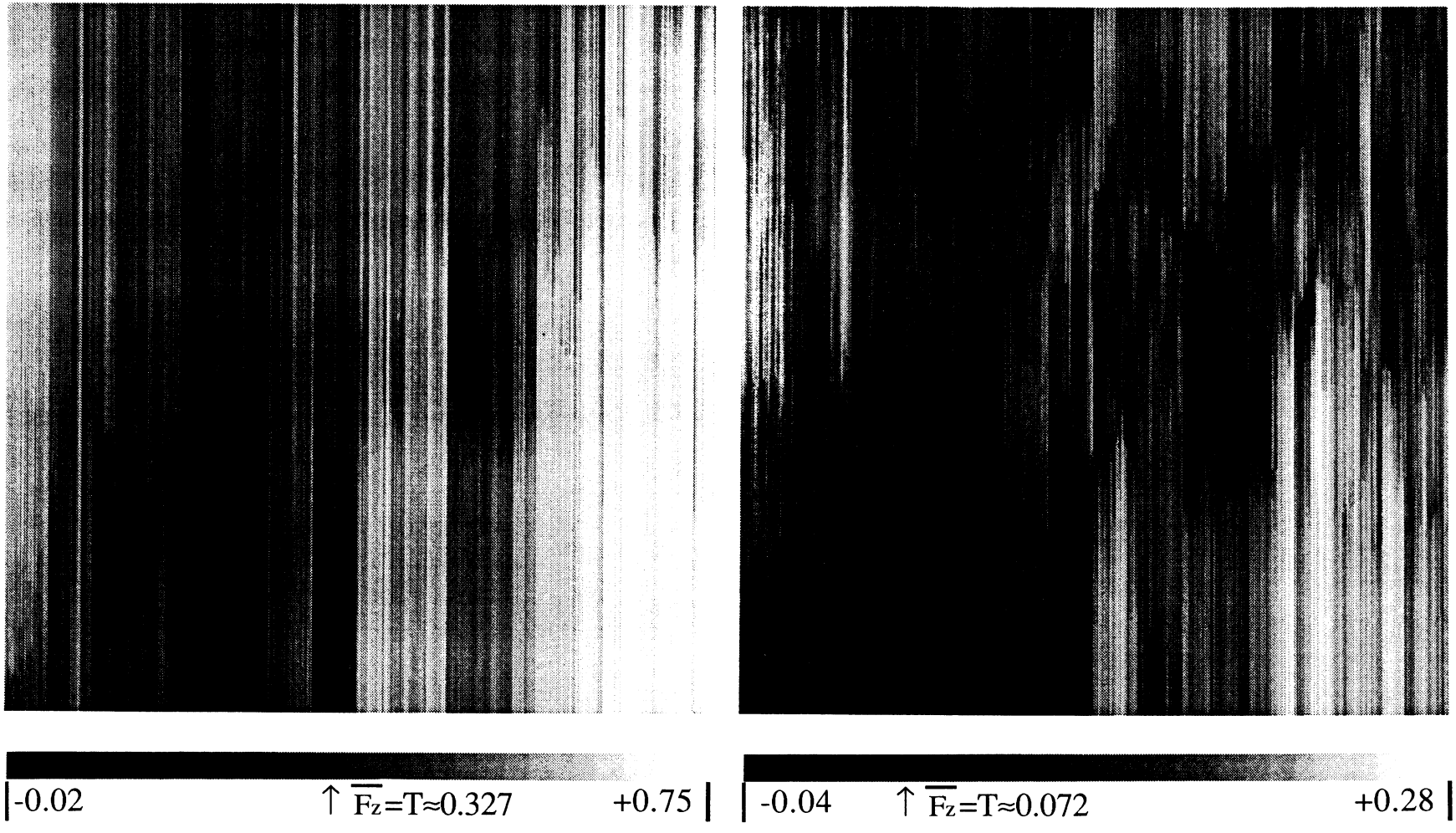

Figs. 7. Non-diffusive (eigenvector) component of DA radiance fields (X):

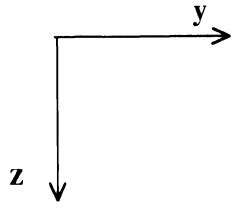

(a) $\overline{\tau}$ = 12.2 (or $\log_2\kappa$ = -7),

(b) $\overline{\tau}$ = 195 (or $\log_2\kappa$ = -3).

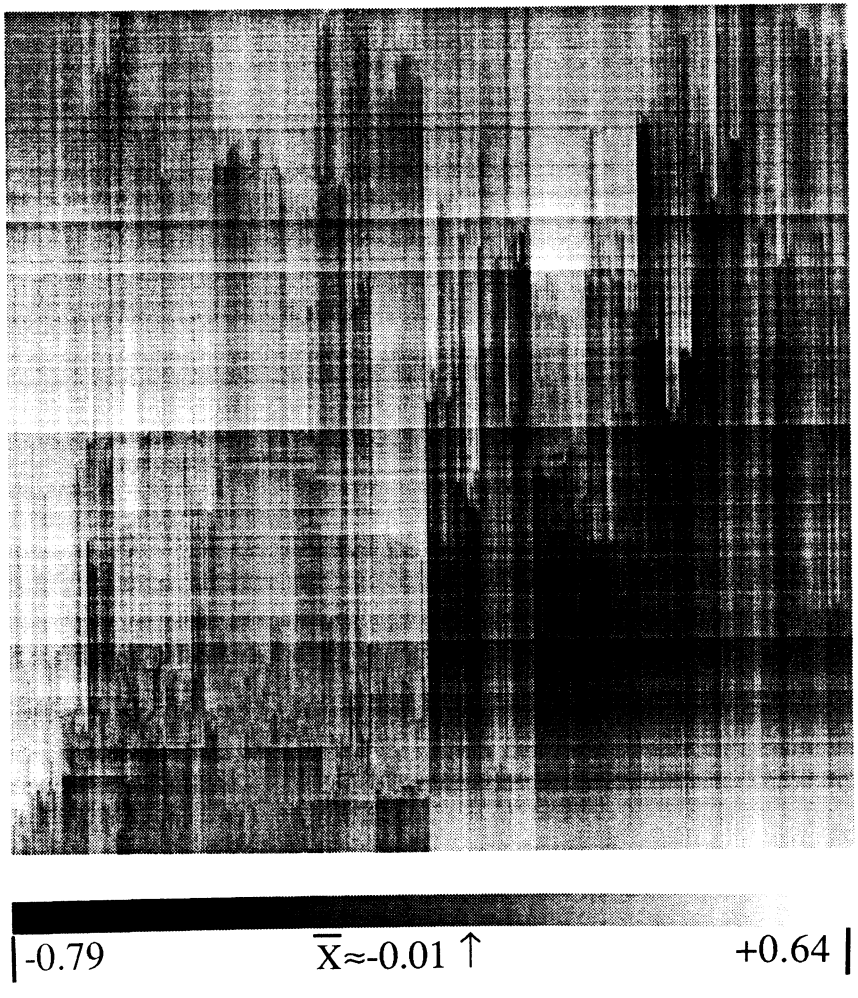

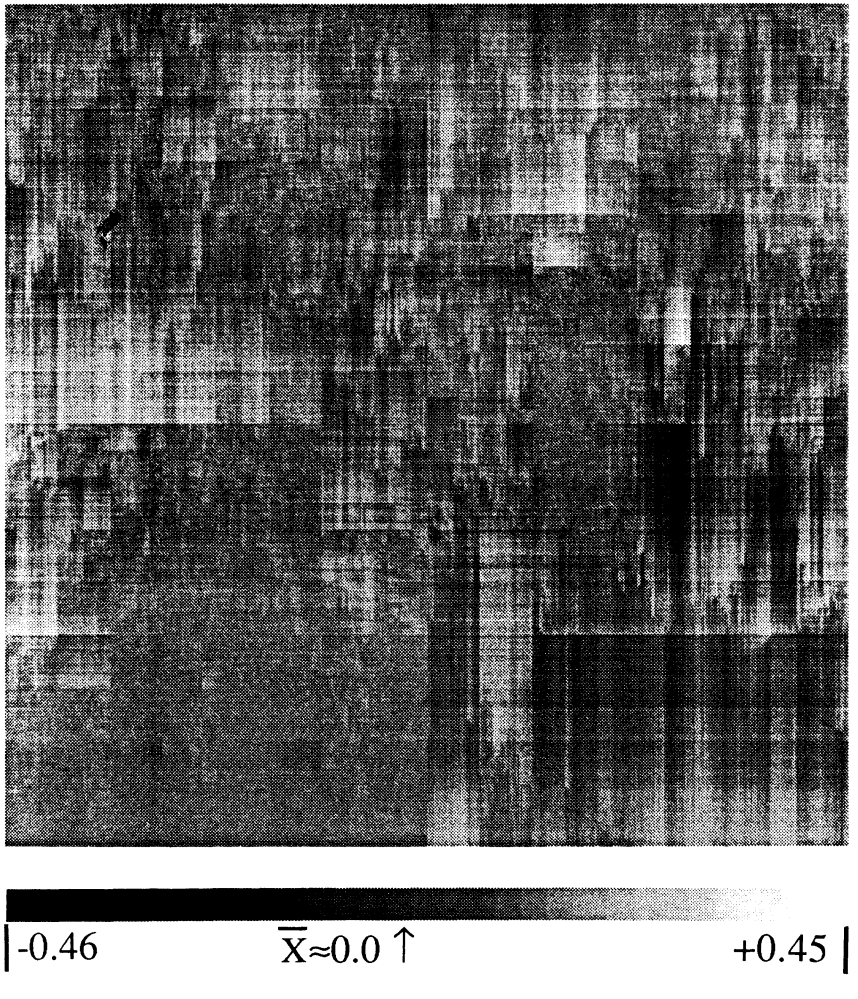

internal total radiance (J) fields for $\overline{\tau}$ = 12.2: before (homogeneous layers) and after (IPs) applying eqs. (30) as well as our full-blown numerical procedure. The *bone fide* plane-parallel profile is very non-representative due to the large concentration of mass in the lower layers of the cloud which, in turn, concentrates radiation in the layers above it. The IP approximation is much closer to reality due to the relatively low mass of the cloud (see §4.6). The orthogonal grid/DA transfer-induced texture of the numerical results has survived the row-averaging to yield local increases in total radiance. (These would not be present in the more relevant ensemble-averaged statistics: on average, the radiant energy will decrease with depth into the cloud but not as predicted by plane-parallel theory, cf. eq. (31), in §4.6.) Of course, the overall top-to-bottom gradient is due to the highly asymmetric vertical BCs that translate illumination (irradiation) from above. However indigenous to cloud-radiation interaction these BCs may be, the asymmetry they impose on the system can be viewed as problematic when trying to understand the more subtle aspects of inhomogeneous transfer some of which may be all but masked in the present situation. Analytical work is in progress on transfer (indeed, simple random walks) in infinite multifractals and, in this context, numerical approaches are also possible if one deals carefully with finite size effects.

In Figs. 5–6, we also notice a "smeared" texture of the net fluxes parallel to the direction they represent (stronger gradients at right angles): the photons are encouraged to stay "on track" until a major obstacle arises or more tenuous regions come within "reach" (a few locally averaged mean free paths $(\kappa\rho(\mathbf{x}))^{-1}$, at most). This collective seeking of the most tenuous optical paths has been called "channeling" in the astrophysical literature.[44] The most obvious manifestation of this can be seen in the lower half of Figs. 5–6 where we witness divergence of horizontal flux on the l.h.s. (above the densest region) and convergence on the r.h.s., simultaneously, we see downwardly decreasing (on the l.h.s.) and increasing vertical fluxes (on the r.h.s.) since the 2-D flow is divergence free due to lack of internal sources (emission) and sinks (absorption). This radiative flow pattern is clearly present at many smaller scales too and quantifying its occurrence statistically is an important task of future research. Notice that the horizontal fluxes are rather narrowly distributed around small negative means and are relatively small in absolute value, $\approx 1/10^{\text{th}}$ of their mean vertical counterpart. These vertical fluxes are distributed around a positive mean which is constrained (by conservation) to be the same in every row from top to bottom and equal to the overall transmittance (T) in eq. (28). The vertical fluxes have by far the strongest fluctuations, ranging from vanishingly small values, in the densest region, to twice T ($\overline{\tau}$ = 12.2) or four times T ($\overline{\tau}$ = 195), in the most tenuous regions. Returning to horizontal fluxes, it is remarkable that such locally small numbers can account for (up to almost) an order of magnitude difference between exact and IP calculations of net overall flux T (see §4.6 below).

Finally, we turn to Figs. 7a–d where we see the much more up/down- and y/z-symmetric "non-diffusive" component defined in eq. (11). By and large, we see that it is most apt to vanish in the most opaque regions/clouds. This is indeed what we expect from standard (continuous angle) theory behind the diffusion approximation which tells us that it works best for quasi-isotropic radiation fields which, in turn, we expect to find in dense regions where lots of scattering occurs (due to shorter-than-average free paths) and as (optically) far from sources/sinks as possible since these produce/cause "streaming" rather than "random walking" photon behavior; in our case, this means top/bottom boundaries. On closer examination however, we see that |X| is rarely negligible compared to T in the thin cloud. In the thick cloud however, it can exceed T (and even $\max F_z$) only very locally but, curiously, quite deep inside. It is noteworthy that recent[45] *in situ* measurements of radiance in extended (marine stratocumulus) cloud decks strongly suggest a predominance of diffusive behavior although $I_{\mathbf{u}}(\mathbf{x})$ was sampled exclusively in a vertical plane, hence only vertical fluxes are accessed. Our results strongly suggest, on the one hand, that in future cloud radiation experimental studies, horizontal fluxes should not be overlooked due to their fundamental role in radiation "channeling" and that, on the other hand, concerted experimental and theoretical efforts should be made to better understand the transitions between the kinetic and diffusion transport regimes as well as try to characterize the situations where the IP approximation work best as it might turn out to be sufficiently accurate for some practical applications.

4.5. The exiting radiation fields, their power- and singularity-spectra

In Figs. 8a,b,c ($\overline{\tau}$ = 12.2) and Figs. 9a,b,c ($\overline{\tau}$ = 195), we have plotted (a) R(y) and T(y) from eqs. (26) –notice the separate scales in Fig. 9, (b) $E_R(k)$, and (c) $E_T(k)$ the (1-D) power spectra of R(y) and T(y) respectively –notice the use of log-log scales. In both the physical- and Fourier-space representations, it is important to distinguish the "signal" of medium's variability in this single realization experiment from the "noise" due to finite photon statistics in the numerics. This can be done by assuming the Poissonian distribution of detection events; for instance, we notice (Fig. 9a) that reflectance can locally become greater than 1; specifically, $\max_y R(y) = R(489l_0) \approx 1.05$ is probably a real exceedence of 1 since the (uncorrelated) noise level for 10^3 photons is $\sqrt{10^{-3}} \approx 3\%$. In homogeneous media, the photon counts across the cloud would be spatially uncorrelated –and their spectrum flat– whereas, in variable media, weak and strong counts will tend to cluster. We have indicated on Figs. 8–9b,c the level of

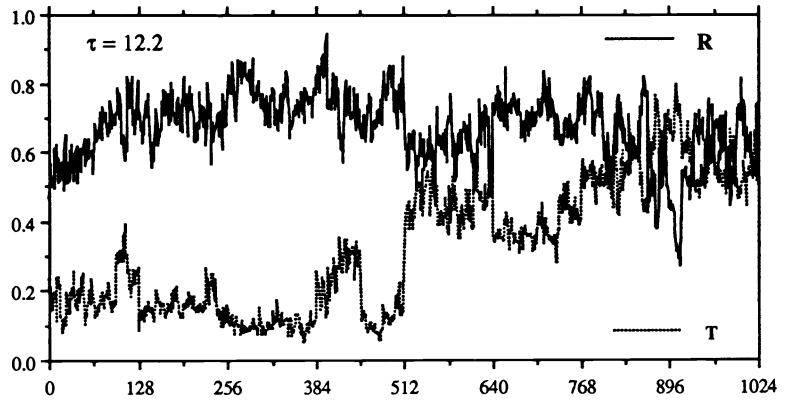

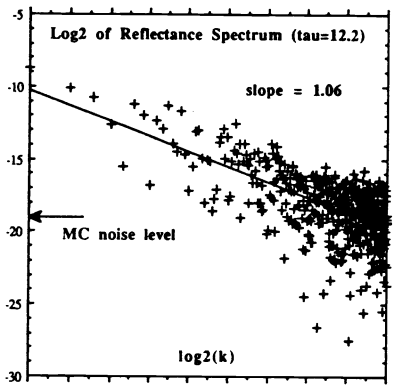

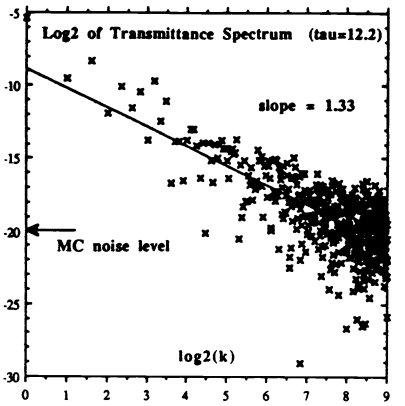

Figs. 8: a) DA reflectance R(y) and transmittance T(y) fields and b), c) their respective power spectra, for $\overline{\tau}$ = 12.2 ($\log_2\kappa$ = -7).

(a) (b) (c)

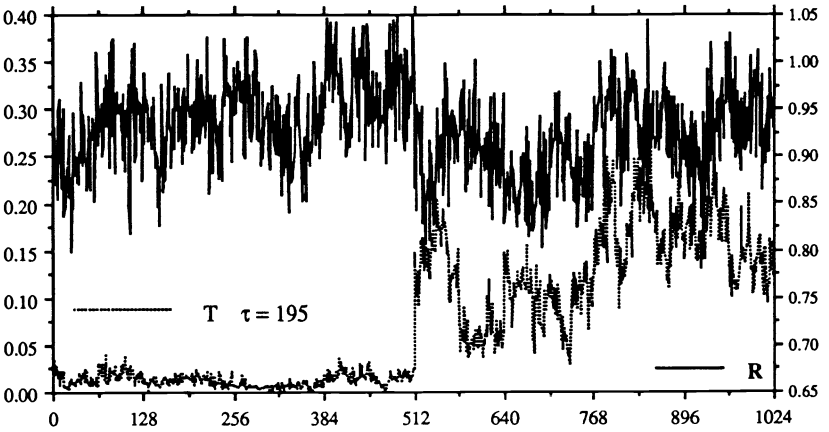

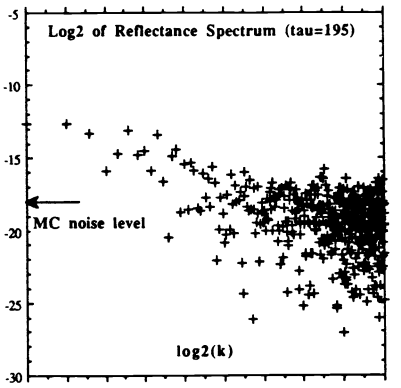

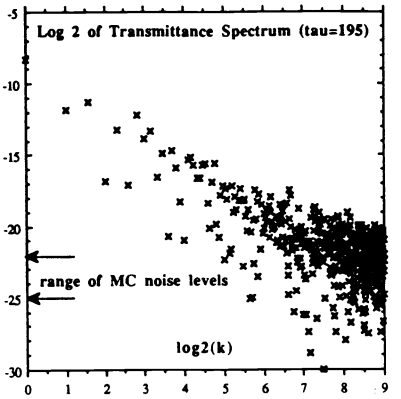

Figs. 9: Same as in Fig. 6 but for $\overline{\tau}$ = 195 ($\log_2\kappa$ = -3).

Monte Carlo noise for the average response (or, in one case, the range of responses) without accounting for potential correlation; since these levels agree with the appearance of any "whitening" trend –mainly in Figs. 9b,c– this cannot be a bad assumption in the circumstances. For the rest (lower k's), we observe spectra that scale very well given the single realization constraint. The spectral exponents for reflectance are around -1, not far from the values found for observed radiances.[46] Transmittance spectra are somewhat steeper due to enhanced energy at the lowest frequencies; this is obviously due to the strong (cloud scale) perturbation of the radiation flow in the lowest layers of the cloud by the very dense region on the l.h.s. By and large, we are not surprized to see how easy it is to obtain *"1/f"*-type spectra –which is another comment (§4.1) on the weakness of this statistic.

Fig. 10 illustrates the smoothing power of enhanced multiple scattering in another way, namely, by showing the codimension functions of the albedo fields; more precisely, we take $c_R(\gamma_R) = -\log_\lambda(dP_R/d\gamma_R)$ from (18) where $\gamma_R(y) = \log_\lambda(R(y)/R)$ from definitions (27), (28) and (17) for $\log_2\kappa = -7,\cdots,-3$. Particularly obvious is the gradual narrowing of the singularity spectrum, i.e., effectively smaller C_1's are to be expected. We also see a simultaneous trend from more skewed distributions to more symmetric ones. This is entirely consistent with the observational finding[47] that very large scale (partly cloudy, GOES) satellite imagery are more monofractal like with $C_1 \approx 0.2$ whereas recent analyses[63] of much smaller scale (90% cloudy, Landsat-MSS) images yield more log-normal like distributions and C_1 values in the range 0.05–0.1. Some insight into the mechanisms of radiative smoothing can be gained by pondering the reasons that make very large reflectance values not only improbable but physically impossible. On the one hand, it is not hard to identify the factors that are limiting R(y): in the IP approximation it is strictly less than 1 so any excess is necessarily due to horizontal fluxes taking energy into regions where it is already in high concentration, at the expense of regions of lower concentrations (by overall conservation), in blatant contradiction with our general expectation from eq. (11). On the other hand, our present maximum R(y) –merely ≈1.05– occurs (i) at maximum $\kappa = 1/8$ hence systematically shorter free photon paths between scatterings, (ii) at a column (#489) straddled by a more-or-less "V" shaped cluster of above-average singularities (cf. Fig. 3a) that lie right at the top of the cloud, a situation where recently injected photons are likely to be "trapped" and reflected, and (iii) this structure happens to be right above the very dense region at the bottom of the cloud, hence further concentration of radiant energy; at present, it is impossible to quantify the contributions of these three factors separately but clearly (i) is perfectly natural from first principles but further enhancement of κ can only bring on still smoother fields, (ii) is certainly not exceptional in these kinds of cloud models, and (iii) is completely circumstantial. Our DA reflectances obviously obey the same conservation rules as continuous angle fluxes in upwards hemisphere while remotely sensed albedoes are really radiances simply related to the equivalent Lambertian reflector; they are therefore not physically bounded but –since fluxes are– very large values call for Fresnelian-like optics (e.g., ocean "glint"), unlikely and unobserved in clouds. This powerful smoothing effect of multiple scattering is reminiscent of the fact that Nature produces clouds that are at once radiatively featureless and highly variable internally: arctic status[48] which were once viewed as potential benchmarks for homogeneous plane-parallel transfer calculations in full angular detail.

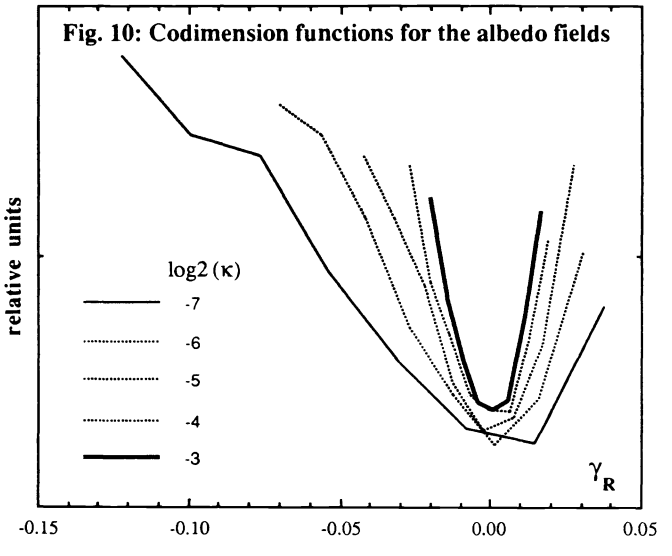

Fig. 10: Codimension functions for the albedo fields

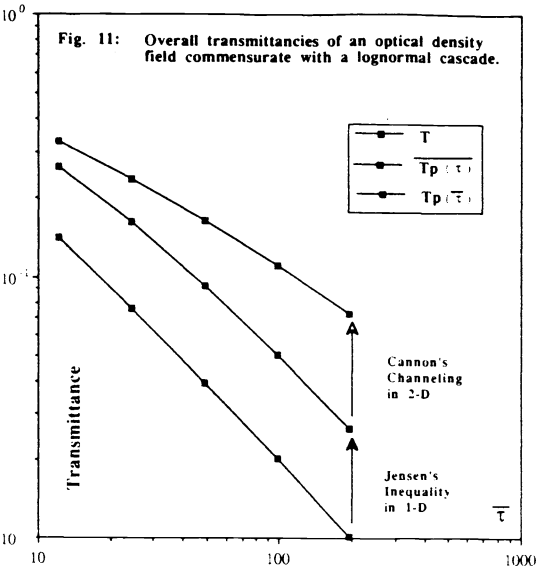

Fig. 11: Overall transmittancies of an optical density field commensurate with a lognormal cascade.

4.6. The remarkable inequalities in overall responses calculated with various assumptions

By showing $T_p(\overline{\tau})$, $\overline{T_p(\tau)}$, and T, as functions of $\overline{\tau} = \kappa\overline{\rho}L$ for $\log_2\kappa = -7,\cdots,-3$, Fig. 11 summarizes many of our findings and rises some interesting questions. It shows that, while spatial albedo variability diminishes in Fig. 10, we see here the gradual enhancement of the radiative effects of inhomogeneity as the degree of multiple scattering (hence nonlinear ρ-I_u coupling) increases. We are not surprized to see that (Jensen's) general inequality $\overline{T_p(\tau)} \geq T_p(\overline{\tau})$ is verified since it is valid for any nonlinear –in this case, concave– function averaged over any p.d.f.[49] More intriguing is the fact that, at first, most of the overall inhomogeneity effect is captured by the IP calculation, implying that most of the photons have probably not travelled very far laterally between injection and escape. As the density increases so is the length (and lateral extent) of the typical photon random walk. "Channeling" is also continuously enhanced while the IP correction to the thoroughly plane-parallel calculation goes to a constant ratio. This is not unexpected since κ only yields a prefactor in our IP analytical calculations discussed elsewhere. Interestingly, the numbers that measure the net horizontal fluxes are (about twice) larger in the thinnest medium than in the thickest (cf. Figs. 5a–b) so the local quantitative characterization of channeling is bound to be quite subtle in theory and in experiments. At $\overline{\tau} \approx 200$, we have reached a whole order of magnitude ratio between plane-parallel and inhomogeneous results for total transmittance; such ratios are in step with the worst discrepancies reported in connection with the cloud albedo paradox: clouds only rarely attain $R \approx 0.9$ (never 0.99!) while optical thicknesses in the hundreds are not unheard of; this alone eliminates the plane-parallel –and otherwise quasi-homogeneous– models in favor of the scaling inhomogeneous ones. The other inequality we observe, $T > T_p(\overline{\tau})$ along with the sharper $T > \overline{T_p(\tau)}$, can be shown to hold in general for diffusive transfer;[42] they are probably also exact within the framework of DA transfer (no counter-examples have been observed yet in spite of extensive numerical experimentation). One can only speculate that, due to the intermediate position of DA transfer ($0 < p < \infty$) within a continuum going from IPs ($p = 0$) to diffusion ($p = \infty$), there exists a further inequality, $T_{diffusion} > T\ (= T_{DA})$; this would allow us to put bounds on both sides of T_{DA}. Turning to ensemble-averages, we can make the following inference using Jensen's inequality alone:

$$\text{If } T \geq T_p(\overline{\tau}) \text{ for every realization, then } \quad \langle T \rangle \geq \langle T_p(\overline{\tau}) \rangle \geq T_p(\langle \overline{\tau} \rangle) = T_p(\langle \tau \rangle). \tag{31}$$

The observed inequalities in Fig. 10 may be generalizable to normal, isotropic or otherwise axisymmetric illumination conditions in continuous angles, conditions that may eventually be relaxed in the very thick cloud regime; but inhomogeneous cloud[50] (or broken cloud fields[51]) that are thin enough are known reflect more –transmit less– than their plane-parallel counterparts at slant enough conditions.

5. CONCLUSIONS, METEOROLOGICAL IMPLICATIONS AND FUTURE DEVELOPMENTS

In this paper, we pursue our investigation into the radiative properties of extremely variable scale-invariant inhomogeneous clouds by moving away from monofractal models towards multifractals and away from spatially unresolved radiation fields towards detailed spatial resolution. Both internal and exiting radiances have thus been computed –within the framework of Discrete Angle (DA) transfer– for an externally illuminated density field generated by a discrete log-normal cascade on a 1024x1024 grid; five different optical thicknesses were obtained from this density field of fixed physical size by using an overall multiplicative factor. To the best of our knowledge, this is the first complete numerical solution of a transfer problem on such a wildly fluctuating medium. The numerics were validated by successfully comparing results from two vastly different techniques (direct Monte Carlo simulation and finite differences followed by relaxation). Apart from providing us with material to test any improvement in numerical methodology, the new results allow us to demonstrate visually and quantitatively the importance of the horizontal fluxes induced by the spatial variability in at least two respects that come hand-in-hand: "channeling" and smoothing.

In a thick homogeneous cloud, the photons that are not more or less immediately reflected are soon performing standard random walks and they can sample a large volume of cloud before exiting but with no preferred regions or directions of propagation: the average flow of radiant energy is a slow downward motion driven by the illumination/lack of- at the top/bottom boundaries. This picture (of straight vertical flux-lines) changes radically in very inhomogeneous cloud: the structure of the radiative flow is chaotic and, while the overall top-to-bottom average gradient necessarily persists, the fluctuations in (optical) density generate severe perturbations in a systematic way. Flux lines will diverge upstream from a denser region, converge into a more tenuous region. This is how "channeling" works and the qualitative description is deliberately made similar to that of liquid flow in porous media.[52] This analogy could be made quantitative if one could always and everywhere model radiation transport within the diffusion (Eddington) approximation. In our simulations, we show that this is not the case and, as expected from first principles,

we have mapped those regions/clouds where one can to the densest but strong departures are observed even in the thickest cloud we studied.

The thicker the cloud, the further the radiation can be transported laterally, as in the homogeneous case. However, contrary to the homogeneous case where there are no spatial fluctuations of density to smooth, we witness here a fluctuation ratio in density of 10^{11} that can be reduced to a 1.05:0.80 ratio in albedo. This is partly due to the physical limits on albedo: in "independent pixel" calculations it can never exceed 1 whereas in full-blown transfer it can, but only locally since total radiant energy flux is conserved, and weakly since fluxes are always competing with concentrations of radiant energy –more so if the concentration is above-average. In our case, the occurrence of >1 albedo is spatially co-located with an obvious favorable fluke in density distribution (but nothing pathological for a multifractal). The other smoothing factor is provided by the horizontal fluxes which need not be comparable to their vertical counterparts in terms of magnitude. Simultaneously, the same horizontal fluxes induce a ten-fold increase in overall transmittance or, equivalently, a ten-fold ratio in apparent-to-true optical thickness with respect to homogeneous plane-parallel calculations. Five-fold ratios are obtained with respect to "inhomogeneous" (independent pixel) plane-parallel calculations where the nonlinearity of the transmittance (or albedo) function of optical thickness is exploited but the contribution of the horizontal fluxes is totally neglected.

This study opens the possibility that horizontal fluxes can be at once locally so small as to be difficult to detect and, at the same time, so important globally that (i) they are paramount in the explanation of the cloud "albedo paradox" (that arises at visible wavelengths when homogeneous transfer models are applied blindly) and (ii) they will probably play an important role in the current debate on the cloud "absorption anomaly" in the near IR.[53] This provides an important reason to improve current *in situ* cloud radiation studies by allowing the measurement of horizontal fluxes as well as vertical fluxes. (This calls for the sampling of radiances from all directions, not just in one meridian plane.) In particular, this would allow us to study the conditions where the 3-D diffusion approximation is applicable to real clouds; furthermore, the doubtful outcome where horizontal fluxes are truly negligible would justify the current use of independent pixel type hypotheses. Simultaneously, accurate and reliable cloud droplet probings are obviously important in order to determine their statistical properties down to the smallest possible scale; this is crucial if we want to focus future transfer studies towards truly realistic variability models. Multiple scaling characterizations of cloud liquid water content are only starting to become feasible.[54] Sooner or later, these will have to incorporate the vertical and azimuthal anisotropies which are so obvious in many cloud-types and this can easily be done within the framework of Generalized Scale Invariance (GSI), in both analysis[55] and synthesis[56] modes.

There are many outstanding problems and conceivable developments in the realm of transport problems in multifractal media, some of which have been stated in the main text. So we will mention only a few more that relate more closely to the numerical aspects of the work presented here. Although using intermediate cascade steps as initial guesses for relaxation purposes is not computationally advantageous, the results are quite interesting and should be studied in their own right as an example of the development of a "radiative" cascade, however thwarted it may be in comparison to those illustrated in our Figs. 2–3a. In turn, this exercise could lead to more insight into the basic physics of scalingly inhomogeneous transfer; moreover, this line of attack on fully resolved radiation fields directly generalizes our previous approach to their unresolved counterparts (where optical thickness is changed by varying the cloud's physical size). Monte Carlo orders-of-scattering statistics could –and should– be exploited to generalize conservative scattering results to conditions with weak absorption which prevail in the near IR where inhomogeneity effects are virtually unexplored at present in spite of their obvious relevance to the important issue of the anomalous absorption in clouds. Finally, the dataset presented in this paper should be not just visualized but quantitatively analyzed for spatial/angular radiance signatures of singularities in the density field whether co-located or offset in space; to this end, scaling vectorial n-point statistics can be defined within the general framework of multifractal formalism.[57]

6. ACKNOWLEDGMENTS

The authors wish to thank B. Watson, R. Borde, D. Lavallée, F. Schmitt, Y. Tessier, R. Davies, I. Graham, M. Grant, G. Austin, P. Gabriel, P. Gauthier and J. F. Geleyn for the fruitful discussion. Extremely generous portions of the CCVR's Cray 2 time where put at our disposal by Météo-France –of this, we are extremely grateful. We also acknowledge the financial support of DOE's Atmospheric Radiation Measurement (ARM) project, contract #DE-FG03-90ER61062. One of us (A.D.) specially acknowledges the DMN/EERM for the opportunity to be *Collaborateur Scientifique* at the CRMD (Paris) in 1990, where and when most of this work was performed, as well as the whole groups of people involved in atmospheric radiation research at CNRM (Toulouse), LOA (Lille), NASA (Goddard Space Flight Center) and AES (Downsview), and who created the necessary conditions for very stimulating visits.

7. REFERENCES

1. Lovejoy, S., A. Davis, P. Gabriel, D. Schertzer, and G. L. Austin, "Discrete Angle Radiative Transfer - Part I: Scaling and Similarity, Universality and Diffusion," *J. Geophys. Res.*, ***95***, 11699-11715, 1990.
2. Gabriel, P., S. Lovejoy, A. Davis, D. Schertzer, and G. L. Austin, "Discrete Angle Radiative Transfer - Part II: Renormalization Approach for Homogeneous and Fractal Clouds," *J. Geophys. Res.*, ***95***, 11717-11728, 1990.
3. Davis, A., P. Gabriel, S. Lovejoy, D. Schertzer, and G. L. Austin, "Discrete Angle Radiative Transfer - Part III: Numerical Results and Atmospheric Applications," *J. Geophys. Res.*, ***95***, 11729-11742, 1990.
4. Davis, A., P. Gabriel, S. Lovejoy, and D. Schertzer, "Asymptotic Laws for Thick Clouds, Dimensional Dependence - Phase Function Independence," in *IRS'88: Current Problems in Atmospheric Radiation*, Eds. J. Lenoble and J. F. Geleyn, 103–106, Deepak Publ., 1989.
5. Wiscombe, W. J., R. M. Welch, and W. D. Hall, "The Effects of Very Large Drops on Cloud Absorption, Part 1: Parcel Models." *J. Atmos. Sci.*, ***41***, 1336-1355, 1984.
6. Gabriel, P., S. Lovejoy, G. L. Austin, and D. Schertzer, "Radiative Transfer in Extremely Variable Fractal Clouds," in *Proceedings of the 6th Conference on Atmospheric Radiation* (Williamsburg, May 12–16), A.M.S., Boston, 1986.
7. Lovejoy, S., "The Area-Perimeter Relation for Rain and Clouds," *Science, **216***, 185–187, 1982
8. Lovejoy, S., and B. B. Mandelbrot, "Fractal Properties of Rain, and a Fractal Model," *Tellus*, ***37A***, 209–232, 1985.
9. Cahalan, R. F., "Overview of Fractal Clouds," in *Advances in Remote Sensing (RSRM'87)*, Eds. A. Deepak *et al.*, 371–389, A. Deepak, Hampton (Va.), 1989.
10. Davis, A., S. Lovejoy, and D. Schertzer, "Radiative Transfer in Multifractal Clouds," in *Scaling, Fractals and Non-Linear Variability in Geophysics*, Eds. D. Schertzer and S. Lovejoy, 303–318, Kluwer, Hingham (Mass.), 1991.
11. Chandrasekhar, S., *Radiative Transfer*, pp. xiv+393, Oxford University Press (reprinted by Dover Publ., New York, 1960), 1950.
12. Chu, M. C., and W. S. Churchill, "Numerical Solution of Problems in Multiple Scattering of Electromagnetic Radiation," *J. Chem. Phys.*, ***59***, 855–863, 1955.
13. Siddal, R. G., and N. Selçuk, "Evaluation of a New Six-Flux Model for Radiative Transfer in Rectangular Enclosures," *Trans. Inst. Chem. Eng.*, ***57***, 163–169, 1979.
14. McKellar, B.H.J., and M.A. Box, "The Scaling Group of the Radiative Transfer Equation," *J. Atmos. Sci.*, ***38***, 1063-1068, 1981.
15. Davis, A., S. Lovejoy, D. Schertzer, P. Gabriel, and G. L. Austin, "Discrete Angle Radiative Transfer Through Fractal Clouds," *Proceedings of the 7th Conference on Atmospheric Radiation* (San Fransisco, July 23–27), A.M.S., Boston, 1990.
16. Stauffer, D., *Introduction to Percolation Theory*, pp. vii+124, Taylor & Francis, London, 1985.
17. Kolmogorov, A. N., "Local Structure of Turbulence in an Incompressible Liquid for Very Large Reynolds Numbers," *Dokl. Akad. Nauk SSSR*, ***30*** (4), 299–303, 1941.
18. Landau, L., and E. M. Lifchitz, *Fluid Mechanics*, (English translation: Pergamon, London, 1962), 1st Russian Edition: 1953.
19. Kolmogorov, A. N., "A Refinement of Previous Hypothesis Concerning the Local Structure of Turbulence in Viscous Incompressible Fluid at High Reynolds Number," *J. Fluid Mech.*, ***13***, 82–85, 1962.
20. Obukhov, A., "Some Specific Features of Atmospheric Turbulence," *J. Geophys. Res.*, ***67***, 3011–3014, 1962.
21. Novikov, E. A., and R. Stewart, "Intermittancy of Turbulence and Spectrum of Fluctuations in Energy Dissipation," *Izv. Akad. Naut. SSSR, Ser. Geofiz.*, ***3***, 408–412, 1964.
22. Mandelbrot, B. B, *Les Objets Fractals: Forme, Hasard et Dimension*, Flammarion, Paris, 1975.
23. Parisi, G., and U. Frisch, "A Multifractal Model of Intermittancy," in *Turbulence and Prdicability in Geophysical Fluid Dynamics and Climate Dynamics*, 84–88, Eds. M. Ghil, R. Benzi, and G. Parisi, North-Holland, 1985.
24. Richardson, L. F., *Weather Prediction by Numerical Process*, Cambridge Un. Press, 1922.
25. Halsey, T. C., M. H. Jensen, L. P. Kadanoff, I. Procaccia, and B. Shraiman, "Fractal Measures and their Singularities; The Characterization of Strange Sets," *Phys. Rev.*, ***A 33***, 1141–1151, 1986.
26. Lavallée, D., D. Schertzer, and S. Lovejoy, "On the Determination of the Codimension Function," in *Scaling, Fractals and Non-Linear Variability in Geophysics*, Eds. D. Schertzer and S. Lovejoy, Kluwer, Hingham (Mass.), 1991.
27. Schertzer, D., and S. Lovejoy, "On the Dimension of Atmospheric Motions," in *Turbulence and Chaotic Phenomena in Fluids*, Ed. Tatsumi, 505-508, Elsevier North-Holland, New York, 1984.
28. Meneveau, C., and K. R. Sreenivasan, "A Simple Multifractal Cascade Model for Fully Developed Turbulence," *Phys. Rev. Lett.*, ***59*** (13), 1424–1427, 1987.
29. Schertzer, D., and S. Lovejoy, "Physically Based Rain and Cloud Modeling by Anisotropic, Multiplicative Turbulent Cascades," *J. Geophys. Res.*, ***92***, 9693–9714, 1987.

30. Schertzer, D., S. Lovejoy, D. Lavallée and F. Schmitt, "Universal Hard Multifractal Turbulence: Theory and Observations," in *Non-linear Dynamics of Structures*, Eds. R. Z. Sagdeev *et al.*, 213–235, World Scientific, Hong Kong, 1991.
31. Lavallée, D., D. Schertzer, and S. Lovejoy, "Universal Multifractals, Theory and Observations of Land and Ocean Surfaces and Clouds," *S.P.I.E. Proceedings*, ***1558***, this volume, 1991.
32. Corssin, S., "On the Spectrum of Isotropic Temperature Fluctuations in Isotropic Turbulence," *J. Appl. Phys.*, ***22***, 469–473, 1951.
33. Obukhov, A., "Structure of the Temperature Field in a Turbulent Flow," *Izv. Akad. Naut. SSSR, Ser. Geogr. I Geofiz.*, ***13***, 55–69, 1949.
34. Wilson, J., D. Schertzer, S. Lovejoy, "Continuous Multiplicative Cascade Models of Rain and Clouds," in *Scaling, Fractals and Non-Linear Variability in Geophysics*, Eds. D. Schertzer and S. Lovejoy, 185–207, Kluwer, Hingham (Mass.), 1991.
35. Monin, M. A., and A. M. Yaglom, *Statistical Fluid Dynamics, vol. II*, MIT Press, Boston, 1975.
36. Welch, R. M., S. Cox, and J. Davis, "Solar Radiation and Clouds," *Meteorol. Monogr.*, ***39***, 1980.
37. Titov, G. A., "Statistical Description of Radiation Transfer in Clouds," *J. Atmos. Sci.*, ***47***, 24–38, 1990.
38. Boissé, P., "Radiative Transfer Inside Clumpy Media: The Penetration of UV Photons Inside Molecular Clouds," *Astron. Astrophys.*, ***228***,483–502, 1990.
39. McKee, T. B., and J. T. Cox, "Scattering of Visible Light by Finite Clouds," *J. Atmos. Sci.*, ***31***, 1885–1892, 1974.
40. Davies, R., "The Effect of Finite Geometry on Three Dimensional Transfer of Solar Irradiance in Clouds," *J. Atmos. Sci.*, ***35***, 1712–1724, 1978.
41. Glazov, G. N., and G. A. Titov, "Randomization of the Equation for Mean Radiance in Broken Cloudiness," in *Monte Carlo Methods in Computational Mathematics and Mathematical Physics, v. 2*, Computer Center SB USSR Acad. Sc., 41-50, 1979.
42. Davis, A., *Radiation Transport in Scale Invariant Optical Media*, PhD thesis, McGill Un., Physics Dpt., 1991 (in preparation).
43. Stephens, G. L., "Radiative Transfer Through Arbitrarily Shaped Media - Part 1: General Theory, - Part 2: Group Theory and Closures," *J. Atmos. Sci.*, ***45***, 1818–1848, 1988.
44. Cannon, C. J., "Line Transfer in Two Dimensions," *Astrophys. J.*, ***161***, 255–264, 1970.
45. King, M. D., L. F. Radke, and P. V. Hobbs, "Determination of the Spectral Absorption of Solar Radiation by Marine Stratocumulus Clouds from Airborne Measurements within Clouds," *J. Atmos. Sci.*, ***47***, 894–907, 1990.
46. Cahalan, R. F., and J. B. Snider, "Marine Stratocumulus Structure," *Remote Sens. Environ.*, ***28***, 95–107, 1989.
47. Lovejoy, S., and D. Schertzer, "Multifractals, Universality Classes and Satellite and Radar Measurements of Cloud and Rain Fields," *J. Geophys. Res.*, ***95***, 2021–2034, 1990.
48. Tsay, S. and K. Jayaweera, "Characteristics of Arctic Stratus Clouds," *J. Climate Appl. Meteor.*, ***23***, 584-596, 1984.
49. Hardy, G. H., J. E. Littlewood, and G. Pólya, *Inequalities*, Cambridge University Press, London, 2nd ed., 1952.
50. Stephens, G. L., "Radiative Transfer in Spatially Heterogeneous, Two-Dimensional Anisotropically Scattering Media," *J. Quant. Spectrosc. Radiat. Transfer*, ***36***, 51–67, 1986.
51. Kobayashi, T., "Parameterization of Reflectivity for Broken Cloud," *J. Atmos. Sci.*, ***45***, 3034–3045, 1988.
52. Cushman, J. H. (Ed.), *Dynamics of Fluids in Hierarchical Porous Media*, pp. xvii+505, Academic Press, London, 1990.
53. Stephens, G. L., and S. Tsay, "On the Cloud Absorption Anomaly," *Q. J. R. Meteorol. Soc.*, ***116***, 671–704, 1990.
54. Durouré, C., and B. Guillemet, "Analyse des Hététrogenéités Spatiales des Stratocumulus et Cumulus," *Atmos. Res.*, ***25***, 331–350, 1990.
55. Pflug, K., S. Lovejoy, and D. Schertzer, "Generalized Scale Invariance, Differential Rotation and Cloud Texture," in *Nonlinear Dynamics of Structures*, Eds. R. Z. Sagdeev *et al.*, 71–80, World Scientific, Hong Kong, 1991.
56. Schertzer, D., and S. Lovejoy, "Generalized Scale Invariance in Turbulent Phenomena," *P.C.H. Journal*, ***6***, 623–635, 1985.
57. Schertzer, D., and S. Lovejoy, "Scaling Nonlinear Variability in Geodynamics: Multiple Singularities, Observables and Universality Classes," in *Scaling, Fractals and Non-Linear Variability in Geophysics*, Eds. D. Schertzer and S. Lovejoy, 41–82, Kluwer, Hingham (Mass.), 1991.
58. Schuster, A., "Radiation Through a Foggy Atmosphere," *Astrophys. J.*, ***21***, p. 1, 1905.
59. Meador, W. E., and W. R. Weaver, "Two-Stream Approximations to Radiative Transfer in Planetary Atmospheres: A Unified Description of Existing Methods and a New Improvement," *J. Atmos. Sci.*, ***37***, 630–643, 1980.
60. Falconer, K. J., *Fractal Geometry - Mathematical Foundations and Applications*, pp. xxii+288, J. Wiley, New York, 1990.
61. Preisendorfer, R.W., *Hydrological Optics*, 8 vols., NOAA-ERL, Boulder, Co., 1976.
62. van de Hulst, H.C., and K. Grossman, "Multiple Light Scattering in Planetary Atmospheres," in *The Atmospheres of Venus and Mars*, edited by J.C. Brandt and M.B. McElroy, 35–55, Gordon and Breach, New York, 1968.
63. Tessier, Y., S. Lovejoy, and D. Schertzer, "Universal Multifractals: Theory and Observation for Rain and Clouds," submitted to *J. Appl. Meteor.*, 1991.